Industrial Crops & Products 233 (2025) 121484

Contents lists available at ScienceDirect

Industrial Crops & Products

journal homepage: www.elsevier.com/locate/indcrop

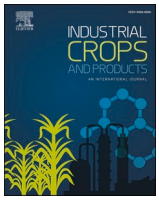

Connecting chemical and biological properties to identify new functional materials: A study on *Trifolium nigrescens* extracts

Milena Terzic [a], Gokhan Zengin [b,*], Andrei Mocan [c,*], Oleg Frumuzachi [c], Mehmet Veysi Cetiz [d], Giovanni Caprioli [e], Laura Acquaticci [e], Simone Angeloni [e], Ismail Senkardes [f], Enver Saka [b], Florinda Fratianni [g], Francesca Coppola [g,h], Filomena Nazzaro [g]

[a] Faculty of Technology Novi Sad, University of Novi Sad, Novi Sad, Serbia
[b] Department of Biology, Faculty of Science, Selcuk University, Konya 42130, Turkey
[c] Department of Pharmaceutical Botany, "Iuliu Haţieganu" University of Medicine and Pharmacy, Gheorghe Marinescu Street 23, Cluj-Napoca 400337, Romania
[d] Department of Medical Biochemistry, Faculty of Medicine, Harran University, Sanliurfa 63290, Turkey
[e] Chemistry Interdisciplinary Project (ChIP), School of Pharmacy, University of Camerino, Via Madonna delle Carceri 9/B, I-, Camerino, MC 62032, Italy
[f] Deparment of Pharmaceutical Botany, Faculty of Pharmacy, Marmara University, Istanbul, Turkey
[g] Institute of Food Science, CNR-ISA, Via Roma 64, Avellino 83100, Italy
[h] Department of Agricultural Sciences, University of Naples Federico II, Piazza Carlo di Borbone 1, Portici (NA) 80055, Italy

ARTICLE INFO

Keywords:
Trifolium nigrescens
Docking
Molecular dynamics
Extraction
Antioxidant
Enzyme inhibition
Anti-biofilm activity

ABSTRACT

In this study, extracts of the plant species *Trifolium nigrescens* collected in Turkey were examined. The extracts were obtained by maceration as a conventional method for the extraction of bioactive metabolites, using solvents of different polarity (ethyl acetate, ethanol, 70 % ethanol and water). The antioxidant, enzyme inhibitory and anti-biofilm potential was investigated using *in vitro* assays, as well as chemical profiles. Ellagic acid was the dominant phenolic acid (4115.87 mg/kg), delphinidin-3-galactoside was the most abundant anthocyanin (24789.25 mg/kg), while hyperoside as flavonoid was identified in the highest concentration (42450.94 mg/kg). Ethanol and 70 % ethanol were the most effective extracts in the radical scavenging and reducing power assays. However, the metal chelating abilities of the ethyl acetate (14.80 mg EDTAE/g) and 70 % ethanol (14.13 mg EDTAE/g) extracts were close to each other. In terms of AChE and tyrosinase inhibition, 70 % ethanol was the most active with these values of 2.34 mg GALAE/g and 48.97 mg KAE/g, respectively. Based on the microbiological aspects, the extracts were able to inhibit the mature biofilm or act on the metabolism of their sessile cells, with the percentage of inhibition reaching almost 60 %. In some cases, such as in the evaluation of anti-biofilm activity against *Acinetobacter baumannii,* the presence of water in the extract buffer had a positive effect on the inhibition of mature biofilm. Furthermore, molecular docking and 100-ns molecular dynamics simulations were conducted to assess the interaction of selected compounds with both microbial proteins and all five standard enzymes. The correlation analysis identified some polyphenols, including phenolic acids and flavonoids, which were most involved in enhancing or attenuating the antibiofilm effect of the extracts.

1. Introduction

Medicinal plants have played an important role in traditional medicine as they offer therapeutic properties for the treatment of various pathological conditions. The use of medicinal plants for healing and health has prevailed across cultures and centuries, and continues today in various forms, from traditional herbal medicines to pharmaceutical formulations (Elkordy et al., 2021). With the development of phytotherapy in modern medicine, plants have been integrated into various pharmaceutical forms, and the development of herbal medicines is intensifying. Contrarily, nutraceuticals and dietary supplements occupy an important place in the wellness industry, and numerous plants are used in the development and formulation of dietary supplements (Chopra et al., 2022). Integration into modern medicine requires scientific validation, which would confirm the efficacy and safety of herbal medicines, sustainability, which requires limited access to medicinal plants to preserve biodiversity, and regulation and standardization, which herbal medicines must undergo to ensure quality and dosage

* Corresponding authors.
E-mail addresses: gokhanzengin@selcuk.edu.tr (G. Zengin), mocan.andrei@umfcluj.ro (A. Mocan).

https://doi.org/10.1016/j.indcrop.2025.121484
Received 14 April 2025; Received in revised form 27 June 2025; Accepted 6 July 2025
Available online 10 July 2025

(Balkrishna et al., 2024; Frumuzachi et al., 2025).

The genus *Trifolium* belongs to the Fabaceae family and is commonly known as clover. Plant species of this genus are widespread, even in urban and rural areas, and are mostly used as animal feed (Demirkiran et al., 2013). The genus *Trifolium* is important for the ecosystem as the species of this genus are very rich in pollen for honey production (Keskin, 2024). This genus is widespread in the Mediterranean region, especially in Turkey, where 103 species of this genus have been identified (Demirkiran et al., 2013). From an economic and agricultural point of view, the most commonly used and very important plant species of this genus are *T. repens* (white clover), *T. pratense* (red clover), *T. nigrescens*, *T. arvense*, *T. hybridum*, *T. resupinatum*, *T. alpinum*, *T. thalii*, *T. alexandrinum*, *T. subterraneum*, *T. badium* and *T. ochrole* (Kolodziejczyk-Czepas et al., 2014).

In traditional medicine, plant species of the genus *Trifolium* are used for the treatment of eczema, psoriasis and rheumatic diseases, but are also known as painkillers, antiseptics and expectorants (Kolodziejczyk-Czepas, 2012). Modern pharmacological studies have confirmed that *Trifolium* species exhibit a wide range of biological activities, including antioxidant, anti-inflammatory, antimicrobial, cytotoxic, estrogenic, and anticancer effects (Kolodziejczyk-Czepas, 2016). These biological effects are primarily attributed to the presence of various bioactive compounds such as isoflavones (e.g., formononetin, biochanin A, daidzein, genistein, glycitein), flavonoids (e.g., quercetin, kaempferol, myricetin), phenolic acids (e.g., caffeic acid, chlorogenic acid, rosmarinic acid), and volatile compounds (e.g., (*E*)-3-hexenyl acetate, β-phellandrene, lilac aldehyde) (Kolodziejczyk-Czepas, 2016; Sultana et al., 2022).

T. nigrescens, commonly known as small white clover, is an annual species broadly distributed across the Mediterranean region, including parts of North Africa and the Middle East. Although it shares the characteristic white flower heads with *T. repens*, *T. nigrescens* differs in being an annual plant, while *T. repens* is a creeping perennial that establishes roots at its nodes. Additionally, *T. nigrescens* produces smaller inflorescences (Keith, 2013). In a study conducted by Demirkiran et al. (2013), the chemical profile of *T. nigrescens* subsp. *petrisavi* was explored for the first time. Bioassay-guided fractionation of its ethyl acetate leaf extract led to the identification of a novel biflavone, along with eleven known compounds, including phenolics and flavonoid glycosides. Structural elucidation was accomplished through comprehensive NMR and MS analyses. Several of the isolated compounds demonstrated strong antioxidant capacity and significant tyrosinase inhibitory activity. The new biflavone also showed superior antioxidant activity compared to α-tocopherol in DPPH and ABTS scavenging assays.

Despite these promising results, no further studies were conducted on this species. Therefore, this study aimed to investigate the phytochemical profile and biological potential of *T. nigrescens* extracts obtained using solvents of varying polarity. Antioxidant, enzyme inhibitory, and antibiofilm activities were assessed, and molecular docking alongside 100-ns molecular dynamics simulations were employed to further explore the interaction of key compounds with microbial and metabolic targets, highlighting their relevance for pharmaceutical and food applications.

2. Materials and methods

2.1. Plant material and extraction methods

In 2023, a plant sample collection was conducted in Maltepe, Istanbul (Turkey). Botanist Dr. Ismail Senkardes carefully performed the taxonomic identification of the specimens that were obtained. For future use and confirmation, a voucher specimen (voucher number: MARE 22671) was formally placed at the Marmara University, Pharmacy Faculty herbarium. Aerial parts were meticulously separated after gathering and allowed to dry in the shade at room temperature. The dried material was then finely ground into powder using a standardized process. To prevent degradation and ensure long-term stability, the powdered plant material was stored in light-proof containers under controlled conditions.

Four different solvents were used in the extraction process: ethanol, water, a 70 % ethanol/water combination, and ethyl acetate. The extraction process was separately performed for each solvent. Before initiating the extraction process, the plant materials underwent extraction with n-hexane in a Soxhlet apparatus for 5 h to eliminate lipophilic substances. After the process, a 10-gram sample was macerated with 200 milliliters of ethanol, ethyl acetate, and an ethanol-water mixture for 24 h at room temperature. To prepare the aqueous extract, 10 g of the plant material were infused with water heated to nearly 80 °C for 15 min. The resultant aqueous extract was freeze-dried after the organic solvents were eliminated using low-pressure evaporation.

2.2. Assay for total phenolic and flavonoid content

Our earlier work examined total phenolics and flavonoids (Slinkard and Singleton, 1977). Folin-Ciocalteu and $AlCl_3$ assays were performed for quantifying these components, respectively. Gallic acid (GA) and rutin (R) were utilized as reference standards in the experiments, and the results were presented as gallic acid equivalents (GAE) and rutin equivalents (RE).

2.3. Metabolomic analysis using LC-MS/MS

Metabolomic analyses were carried out utilizing an Agilent 1290 Infinity II liquid chromatography (LC) system and an Agilent 6546 LC-MS/MS mass spectrometer (Agilent, USA) equipped with an electrospray ionization (ESI) source operating in negative and positive ionization modes. Metabolite separation was done with a Poroshell 120 EC-C18 column (2 × 150 mm, 2.7 μm, Agilent, USA). Detection was performed in the dynamic-multiple reaction monitoring (dynamic-MRM) mode, and the dynamic-MRM peak areas were integrated for quantification. The most abundant product ion was used for quantitation, and the others for qualification. The specific time window for each compound (Δ retention time) was set at 2 min. The supplementary materials provide all the analytical details.

2.4. Assays for in vitro antioxidant capacity

Antioxidant assays were performed as previously described (Grochowski et al., 2017). Trolox equivalents (TE) per gram were calculated for radical scavenging with FRAP, CUPRAC, DPPH, and ABTS. The antioxidant potential was determined in millimoles of TE per gram of extract using the phosphomolybdenum (PBD) assay, and the metal chelating activity (MCA) was quantified in EDTAE.

2.5. Inhibitory effects against some key enzymes

Samples were subjected to enzyme inhibition tests using the following methods (Grochowski et al., 2017): milligrams of galanthamine equivalents (GALAE) inhibited AChE and BChE, while acarbose equivalents (ACAE) per gram of extract inhibited amylase and glucosidase. Tyrosinase inhibition was measured in milligrams of kojic acid equivalents per gram of extract.

2.6. Antibacterial test

The antibacterial properties of the samples were evaluated against both Gram-negative strains (*Acinetobacter baumannii* ATCC 19606, *Pseudomonas aeruginosa* DSM 50071, and *Escherichia coli* DSM 8579) and Gram-positive strains (*Listeria monocytogenes* ATCC 7644 and *Staphylococcus aureus* subsp. aureus ATCC 25923). These bacterial cultures were sourced from the Leibniz Institute DSMZ (Braunschweig Science Campus Braunschweig-Süd, Germany). Prior to testing, bacterial suspensions

were cultivated in Luria Broth for 18 h under continuous shaking at 80 rpm (using a Corning LSE incubator, Pisa, Italy). Incubation temperatures were maintained at 37°C for all strains except *A. baumannii*, which was grown at 35°C.

2.7. Minimal inhibitory concentration (MIC)

The minimal resazurin microtiter plate assay was utilized to determine the MIC, following established protocols (Fratianni et al., 2023; Sarker et al., 2007). The assay was conducted in flat-bottomed 96-well microplates, incubated at 37 °C for 24 h, except for *A. baumannii*, which was incubated at 35 °C under identical conditions. Sterile DMSO served as the negative control, while tetracycline (1 mg/mL in DMSO) was used as the positive control. Each determination was performed in triplicate, and the results were reported as the arithmetic mean ± standard deviation.

2.8. Effect of the extracts on mature biofilm

We followed the protocol of Fratianni et al. (2023). Ten microliters of overnight bacterial cultures, adjusted to 0.5 McFarland standard with fresh Luria-Bertani broth, were added to flat-bottomed 96-well microplates to achieve a final volume of 250 µL per well. The microplates were sealed with parafilm tape to prevent evaporation and incubated at 37 °C (or 35 °C for *A. baumannii*) for 24 h. After incubation, planktonic cells were removed. The extracts were tested at two concentrations, 10 µg/mL and 20 µg/mL, in Luria-Bertani broth to maintain a final volume of 250 µL per well. The plates were incubated for an additional 24 h. The inhibitory percent value was calculated with respect to the control (bacterial cells grown without the presence of the samples, of which the inhibition rate was assumed = 0 %). Triplicate tests were performed, and the results were expressed as the mean ± SD.

2.9. Effect of the extracts on the metabolic activity of sessile cells in mature biofilm

The impact of the extracts at concentrations of 10 µg/mL and 20 µg/mL, added after 24 h, was evaluated by assessing the metabolic activity of sessile bacterial cells. The metabolic activity was measured using the MTT colorimetric assay (Fratianni et al., 2023). As for the crystal violet assay, after incubation, planktonic cells were removed. The extracts were added at two concentrations, 10 µg/mL and 20 µg/mL, in Luria-Bertani broth to maintain a final volume of 250 µL per well. The plates were incubated for an additional 24 h, then planktonic cells were discarded. Subsequently, 150 µL of PBS and 30 µL of 0.3 % MTT (Sigma, Milan, Italy) were added to each well, and the plates were incubated at 37 °C (or 35 °C, depending on the bacterial strain) for 2 h. The MTT solution was then removed, and the wells were washed twice with 200 µL of sterile PBS. Finally, 200 µL of DMSO was added to dissolve the formazan crystals, and absorbance was measured at 570 nm using a Cary 50 Bio Varian spectrophotometer after 2 h. The inhibitory percent value on the sessile cells metabolism was calculated with respect to the control (bacterial cells grown without the presence of the samples, for which the inhibition rate was assumed = 0 %). Triplicate tests were performed, and the results were expressed as the mean ± SD.

2.10. Protein and ligand preparation

Molecular docking analysis was carried out to gain insights into the interaction of the major phytochemicals in the extract of *Trifolium nigrescens*. All 3D structures of selected proteins were downloaded from the Protein Data Bank (PDB) (https://www.rcsb.org/) by searching with their respective PDB IDs: Acetylcholinesterase (AChE; PDB ID: 7E 3 H) (Dileep et al., 2022), butyrylcholinesterase (BChE; PDB ID: 6EQP) (Rosenberry et al., 2017), α-amylase (PDB ID: 2QV4), tyrosinase (PDB ID: 2QV4) was retrieved instead. Similarly, a homology model of human glucosidase enzyme (PDB ID: 7KBJ) was sourced from a previous study (Chiavaroli et al., 2023). ***Listeria monocytogenes***: InlA (PDB ID: 1O6T) (Schubert et al., 2002), PI-PLC (PDB ID: 1AOD) (Moser et al., 1997), PrfA (PDB ID: 6EXL) (Kulen et al., 2018), InlB (PDB ID: 4J4L), InlC (PDB ID: 1XEU) (Ooi et al., 2006), InlJ (PDB ID: 3BZ5) (Bublitz et al., 2008), LLO (PDB ID: 4CDB) (Köster et al., 2014), InlH (PDB ID: 1H62) (Barna et al., 2001), MurA (PDB ID: 3R38), IspD (PDB ID: 3F1C). ***Staphylococcus aureus***: DHPS (PDB ID: 1AD4) (Hampele et al., 1997), ParE similar to Gyrase B (PDB ID: 4URN) (Lu et al., 2014), PBP4 (PDB ID: 5TW8) (Alexander et al., 2018), RpsC (PDB ID: 5TCU) (Belousoff et al., 2017), MurE (PDB ID: 4C13) (Wang et al., 2021). ***Acinetobacter baumannii:*** LpxA (PDB ID: 4E6U) (Badger et al., 2012), EPSP synthase (PDB ID: 5BUF) (Sutton et al., 2016), Beta lactamase (PDB ID: 5L2F) (June et al., 2016), GImU (PDB ID: 5VMK), CsuC (PDB ID: 6FJY), CsuE_POSE-1 (PDB ID: 6FJY), CsuE_POSE-2 (PDB ID: 6FJY) (Pakharukova et al., 2018), OBfmR (PDB ID: 6BR7), OmpA (PDB ID: 3TD3) (Park et al., 2012), OXA-23 (PDB ID: 4K0W) (Kaitany et al., 2013), OXA-51 (PDB ID: 5KZH) (Kaitany et al., 2013), OXA-58 (PDB ID: 4OH0) (Smith et al., 2014), and OXA-231 (PDB ID: 6NZ8) (Antunes et al., 2019). Furthermore, all 3D structures of ligands were downloaded from the PubChem database (https://pubchem.ncbi.nlm.nih.gov/) and optimized using Avogadro v1.2.0. All ligand and protein prepare for docking by AutoDock v4.2.6 (Trott and Olson, 2010).

2.11. Docking grid and parameters

The docking grid files were generated either from the literature or using POCASA v1.1 (https://g6altair.sci.hokudai.ac.jp/g6/service/pocasa/). AChE (-54.44, Y: 32.9, −28.65), BChE (32.16, −16.33, 40.73), amylase (17.984, 21.30, 49.36), tyrosinase (21.81, 12.22, 91.40), glucosidase (-18.79, 2.18, 15.75), amylase (14.188, 48.964, 22.886; 28 ×28 ×24 Å) The grid box dimensions were set to 25 × 25 × 25 Å for all targets except amylase (Llorent-Martínez et al., 2025; Yagi et al., 2025). *Listeria monocytogenes*: PI-PLC (30.236, 37.512, 21.541; 64 ×94 ×108 Å), PrfA (-17.276, −14.527, 9.533; 40 ×40 ×40 Å), InlA-Pose-1 (-7.839, 15.509, 64.698; 88 ×70 ×50 Å), InlA-Pose-2 (-5.921, −11.917, 4.481; 88 ×70 ×50 Å), inlB (-11.043, 4.967, −23.943; 62 ×46 ×78 Å), inlC (23.703, 23.065, 15.047; 50 ×40 ×26 Å), InlJ (79.807, −12.073, −97.841; 40 ×40 ×40 Å), LLO (-6.104, 22.138, −52.133; 100 ×76 ×100 Å), inlH (2.075, 9.185, 37.067; 76 ×76 ×76 Å), MurA (18.169, 38.408, 28.905; 54 ×88 ×66 Å), IspD (-16.63, 18.069, −39.052; 90 ×40 ×94 Å). *Staphylococcus aureus*: DHPS (32.46, 6.683, 42.972; 60 ×60 ×60 Å), Gyrase B (31.684, 5.252, 1.572; 60 ×60 X 40 Å), PBP4 (21.390, −62.210, 39.196; 60 ×60 ×60 Å), RpsC (99.46, 230.082, 201.387; 76 ×76 ×76 Å), MurE (-23.122, 2.508, 9.873; 60 ×60 ×60 Å) (Baloglu et al., 2025; Llorent-Martínez et al., 2025; Yagi et al., 2025). *Acinetobacter baumannii:* LpxA (23.713, −33.175, 6.874; 68 ×64 ×70 Å) (Khan et al., 2023). EPSP synthase (5.285, 20.594, −11.817;44 ×62 ×60 Å) (Almihyawi et al., 2022). Beta lactamase (-13.247, −11. 0.88, 37.71; 88 ×84 ×68 Å), GImU (7.735, −39.515, −19.954; 62 ×94 ×110 Å), CsuC (5.565, 26.08, 27.688; 96 ×86 ×122 Å), CsuE_POSE-1 (-17.89, 3.192, 25.11; 74 ×48 ×66 Å), OBfmR (18.244, −5.328, −15.634; 80 ×80 ×84 Å), OmpA (-0.327, 36.645, 14.518; 80 ×40 ×40 Å), OXA-23 (17.378, 1.596, 17.993; 110 ×120 ×116 Å), OXA-51 (22.947, 24.274, 38.505; 76 ×80 ×90 Å), OXA-58 (-13.277, - 1.531, 12.225; 124 ×84 ×60 Å), and OXA-231 (48.677, 122.097, 13.494; 110 ×66 ×82 Å).

2.12. Validation and interaction analysis

Molecular docking studies were conducted using AutoDock Vina v1.1.2 (https://autodock.scripts.edu), with the exhaustiveness parameter set to 32 to ensure comprehensive sampling of ligand conformations (Trott and Olson, 2010). The dimensions of the grid box were meticulously adjusted on the basis of the specific binding sites that were identified within the protein-ligand complexes. To validate the

reliability of the docking protocol, each protein was redocked with its native co-crystallized ligand, and Root Mean Square Deviation (RMSD) values were computed for all atomic coordinates involved (Baloglu et al., 2025; Yildirim et al., 2025). A series of interaction analyses were conducted, with a particular emphasis on hydrogen bonding. These analyses were performed using the Protein-Ligand Interaction Profiler (PLIP) (https://plip-tool.biotec.tu-dresden.de/plip-web/plip/index) (Angeles Flores et al., 2024; Cetiz et al., 2024) to further clarify ligand–protein and enzyme–ligand interactions. To enhance the interpretation and credibility of the docking results, visualization of molecular interactions was conducted through PyMOL v2.5.8 and ChimeraX v1.7.1.

2.13. Molecular dynamics simulations and MM/PBSA free energy calculation

Molecular dynamics (MD) simulations were conducted using the CHARMM GUI platform (https://charmm-gui.org) (Jo et al., 2008; Korpayev et al., 2025). The CHARMM36m force field was utilized for protein parameterization, in accordance with methodologies that had previously been established (Maier et al., 2015). The System preparation followed the established guidelines of the Solution Builder tool (Jo et al., 2008). A periodic boundary box containing TIP3P water molecules was utilized to ensure a minimum separation of 10 Å between the protein and the box edges. Counterions were introduced to maintain electroneutrality and establish a sodium chloride concentration of 0.15 M. Electrostatic and van der Waals interactions were managed using the Verlet cutoff scheme, while bond length constraints were imposed via the Linear Constraint Solver (LINCS) algorithm. Long-range electrostatic interactions were computed using the Particle Mesh Ewald (PME) method. Energy minimization was carried out using the steepest descent algorithm, thereby stabilizing potential energy fluctuations below 1000 kJ/mol/nm. To ensure the stability of the system under investigation, equilibration was performed under both the NVT and NPT conditions at 310 K. The final production simulations spanned 100 nanoseconds using GROMACS 2023.3 (Cetiz et al., 2025). These simulations focused on evaluating the stability, interactions, and therapeutic potential of *A. baumannii-EPSP Synthase_Rutin, A. baumannii-OXA231_Isorhamnetin, A. baumannii-OXA231_Quercetin, L. monocytogenes-InlA_Delphinidin-3–5-diglucoside, L. monocytogenesMurA1_Delphinidin-3–5-diglucoside,* and *S. aureus-MurE_Catechin* complexes complexes. To further quantify ligand-binding affinity and complex stability, a molecular mechanics/Poisson–Boltzmann surface area (MM/PBSA) free energy calculation was performed using the gmx_MPBSA tool (Valdés-Tresanco et al., 2021). The amalgamation of these MD simulations with MM/PBSA calculations engenders a comprehensive understanding of ligand-protein interactions, thereby facilitating the identification of potential inhibitors that exhibit a combination of both strong binding affinity and stability.

2.14. Statistical analysis

Experiments were performed in triplicate, and differences between the extracts were compared using One-way ANOVA (by Tukey's assay) and GraphPad Prism (version 9.2) was used for the analysis. The p value of less than 0.05 was deemed to be statistically significant.

3. Results and discussion

3.1. Total phenolic and flavonoid content of T. nigrescens extracts

The total extractable phenols from the plant species *T. nigrescens* were estimated using a linear gallic acid standard curve. The TPC of all extracts tested ranged from 24.12 to 39.56 mg GAE/g extract. The highest amount of TPC was found in the ethanol extract (39.56 mg GAE/g), followed by the ethanol/water and water extracts (31.01 and 31.08 mg GAE/g extract, respectively). The lowest value was found in the ethyl acetate extract of *T. nigrescens* (24.12 mg GAE/g extract). It was observed that solvents with higher polarity, such as ethanol, ethanol/water (70 %) and water, extracted more phenols than less polar solvents such as ethyl acetate. In this study, the total flavonoid content of the plant species *T. nigrescens* was determined using a linear standard curve for rutin. Like TPC, the ethanol/water extract had a high TFC content (25.68 mg RE/g extract), followed by water (14.09 mg RE/g) and ethanol (6.55 mg RE/g) extracts. The ethyl acetate extract had the lowest TFC content (2.27 mg RE/g (Table 1).

The results of the total phenolic and flavonoid contents investigated in this study are in agreement with the results of the study of the plant species *T. repens* by Kicel and Wolbiś (2013), in which the content of total phenols and flavonoids in flower and leaf extracts was determined. On the other hand, the ethyl acetate extract investigated in this study is a richer source of total phenols than the ethyl acetate extract of the aerial parts of the plant species *T. pratense*. However, the ethyl acetate extract of *T. pratense* had a higher content of total flavonoids than the ethyl acetate extract of *T. nigrescens* (Khorasani Esmaeili et al., 2015). In addition, in the study by Tava et al. (2019), several plant species of the genus Trifolium were analyzed for their total phenolic content. 80% methanol was used as a solvent to obtain the extracts, and an automated accelerated solvent extraction was applied. The plant species *T. repenes*, *T. alpinum* and *T. thalii* were characterized by a lower content of total phenols than the plant species T. nigrescens. On the other hand, *T. alexandrinum*, *T. pratense*, *T. subterraneum*, *T. badium* and *T. ochroleucum* showed a higher content of total phenols compared to *T. nigrescens*. These results could be due to the influence of the chosen extraction solvent, but also to the extraction technique used. In addition, different plant species of the same genus have different contents of bioactive compounds, as the secondary metabolites are present in the plant organs in different concentrations (Mngoma et al., 2025; Sathasivam et al., 2025).

3.2. Phytochemical composition of T. nigrescens extracts

The LC-MS/MS analysis investigated the phytochemical composition of the extracts of *T. nigrescens* and identified 28 phenolic compounds (phenolic acids, anthocyanins, flavonoids) (Table 2). In the ethanol/water extract, ellagic acid, ferulic acid and caffeic acid (4115.87; 698.81 and 1235.59 mg/kg, respectively) were identified in the highest concentrations as derivatives of hydroxycinnamic acids, while gallic acid, chlorogenic acid and neochlorogenic acid were the most abundant in the water extract (40.44; 287.01 and 129.78 mg/kg, respectively). On the other hand, ethyl acetate extract was the richest source of 3-hydroxybenzoic acid and 4-hydroxybenzoic acid (643.75 and 1085.59 mg/kg, respectively). These phenolic acids are derivatives of benzoic acid and are poorly soluble in water, which is why their concentration is highest in the ethyl acetate extract. The high concentration of ellagic acid found in the ethanol/water extract is of great importance due to its pharmacological potential (Najmi et al., 2024). Ellagic acid is a strong regulator of blood glucose levels, which is why it can be used to treat diabetes

Table 1
Total phenolic and flavonoid contents[a] in the tested extracts.

Extracts	TPC (mg GAE/g)[b]	TFC (mg RE/g)[c]
Ethyl acetate	24.12 ± 0.21^{c}	2.27 ± 0.60^{d}
Ethanol	39.56 ± 0.15^{a}	6.55 ± 0.25^{c}
Ethanol/water (70 %)	31.01 ± 0.42^{b}	25.68 ± 0.41^{a}
Water (infused)	31.08 ± 0.14^{b}	14.09 ± 0.24^{b}

differ significantly ($p \leq 0.05$).
[a] values are means ± SD of three measurements, means within each column with different letters (a–d)
[b] mg Gallic acid equivalents per gram of extract
[c] mg Rutin equivalents per gram of extract

Table 2
Chemical characterization* of the tested extracts (mg/kg).

	Compounds	*m/z* molecular ion	EA	Ethanol	Ethanol/Water	Water
1	Gallic acid	169	8.58^{c}±0.5	40.22^{a}±2.4	34.38^{b}±2.1	40.44^{a}±2.4
2	Neochlorogenic acid	353	n.d.	n.d.	153.92^{b}±9.2	287.01^{a}±17.2
3	Chlorogenic acid	353	3.57^{d}±0.2	5.54^{c}±0.3	73.55^{b}±4.4	129.78^{a}±7.8
4	4-Hydroxy benzoic acid	137	643.75^{a}±25.6	434.91^{b}±26.1	359.56^{c}±21.6	304.02^{d}±18.2
5	3-Hydroxy benzoic acid	137	1085.53^{a}±60.1	729.73^{b}±43.8	607.68^{c}±36.5	512.29^{d}±30.7
6	Caffeic acid	179	50.98^{d}±3.0	93.63^{c}±5.6	1235.59^{a}±74.1	1081.23^{b}±64.9
7	Vanillic acid	167	189.00^{a}±11.3	n.d.	n.d.	133.17^{b}±8.0
8	Syringic acid	196.9	23.21^{a}±1.4	17.56^{b}±1.0	n.d.	n.d.
9	*P*-Coumaric acid	1693	180.07^{c}±100.8	116.20^{d}±6.9	289.78^{b}±17.4	421.71^{a}±25.3
10	Ferulic acid	193	163.46^{c}±9.8	120.58^{d}±7.2	698.81^{a}±41.9	445.37^{b}±20.1
11	3,5-Dicaffeoylquinic acid	514.9	n.d.	1.12^{a}±0.1	n.d.	n.d.
12	Ellagic acid	301	1165.02^{d}±60.1	2175.35^{b}±130.5	4115.87^{a}±240.5	1544.04^{c}±92.6
13	*Trans*-cinnamic acid	149	49.28^{a}±3.0	19.73^{b}±1.2	15.43^{c}±0.9	20.63^{b}±1.2
14	Delphinidin 3-galactoside	465.01	22.73^{c}±1.4	10.67^{d}±0.6	30.41^{b}±1.8	45.02^{a}±2.7
15	Delphinidin 3,5 diglucoside	462.9	7456.54^{d}±100.3	12616.73^{c}±702.6	24789.25^{a}±1000.3	21148.96^{b}±60.4
16	Cyanidin−3-glucoside	449	n.d.	n.d.	n.d.	n.d.
17	Petunidin−3-glucoside	479.01	n.d.	3.01^{b}±0.2	8.73^{a}±0.5	n.d.
18	Pelargonidin−3-glucoside	433.01	n.d.	1.46^{c}±0.1	9.72^{a}±0.6	6.12^{b}±0.4
19	Pelargonidin−3-rutinoside	579.01	n.d.	n.d.	n.d.	n.d.
20	Malvidin−3-galactoside	493.01	n.d.	n.d.	n.d.	n.d.
21	Kaempferol−3-glucoside	447	984.87^{d}±50.12	2508.80^{a}±150.5	1744.76^{b}±104.7	1073.55^{c}±64.4
22	Hyperoside	465.01	16166.23^{c}±182.4	2394.75^{d}±143.7	42450.94^{a}±2000.1	27502.82^{b}±1041.1
23	Catechin	289	3.30^{d}±0.1	1741.87^{a}±104.5	84.28^{c}±5.1	337.27^{b}±20.2
24	Epicatechin	289	n.d.	n.d.	n.d.	n.d.
25	Rutin	609	32.21^{d}±1.9	1485.91^{c}±89.1	2695.84^{a}±161.7	1641.97^{b}±98.5
26	Quercetin	300.99	1255.94^{d}±75.4	2312.31^{b}±138.7	3830.99^{a}±229.8	1794.69^{c}±107.7
27	Isoquercitrin	463	8329.48^{d}±400.7	14011.80^{c}±840.7	27645.53^{a}±1010.5	23676.22^{b}±1420.6
28	Phloridzin	435.39	13.89^{d}±0.8	75.28^{a}±4.5	44.83^{b}±2.7	28.98^{c}±1.7
29	Hesperidin	611.01	17.32^{b}±1.0	n.d.	n.d.	912.17^{a}±54.7
30	Isorhamnetin	314.99	26.53^{c}±1.4	41.22^{a}±2.5	38.72^{b}±2.3	15.44^{d}±0.9
31	Kaempferol	287.01	41.07^{d}±2.4	876.84^{a}±52.6	589.15^{b}±35.3	139.85^{c}±8.4
32	Naringin	578.99	n.d.	n.d.	n.d.	n.d.
33	Myricetin	316.99	n.d.	n.d.	n.d.	n.d.
34	Quercitrin	446.99	n.d.	n.d.	n.d.	n.d.
35	Phloretin	272.99	n.d.	n.d.	n.d.	n.d.
36	Resveratrol	227	n.d.	n.d.	n.d.	n.d.
37	Procyanidin A2	575	n.d.	n.d.	n.d.	n.d.
38	Procyanidin B2	576.99	n.d.	n.d.	n.d.	n.d.
	Total polyphenols content		**37912.55^{d}**	**41835.22^{c}**	**111547.70^{a}**	**83242.76^{b}**

nd – not detected
* ±3 SD. Means within each row with different letters (a–d) differ significantly ($p \leq 0.05$).

(Ríos et al., 2018). The available *in vivo* studies have shown that the daily dose of ellagic acid for the treatment of diabetes is 100–200 mg/kg/day (Altamimi et al., 2020). In addition, ellagic acid improves lipid metabolism by lowering triglyceride and LDL cholesterol levels in the blood and increasing HDL cholesterol (Liu et al., 2015). *In vitro* and *in vivo* studies have shown that this phenolic acid also has an exceptional antitumor effect against colon, breast, prostate, lung and melanoma cancer cells, and its presence gives these extracts a special significance. Certainly, this result provides a very good basis for studying the ellagic acid- rich extract in more detail in future research (Ceci et al., 2018). In addition to phenolic acids, anthocyanins were also identified in the extracts of *T. nigrescens*, of which delphinidin-3, 5-diglucoside was the most abundant in all extracts, with the highest concentration found in the ethanol/water extract (24,789.25 mg/kg). Petunidin-3-glucoside and pelargonidin-3-glucoside were also dominant in the ethanol/water extract (8.73 and 9.72 mg/kg, respectively). Ethyl acetate and ethanol extracts were a poorer source of anthocyanins, which is a consequence of the different polarity of the solvents. Due to the polar nature of anthocyanins and the lower polarity of ethyl acetate and ethanol compared to ethanol/water and water, these solvents are not suitable for anthocyanin extraction.

Regarding the presence of flavonoids in the extracts of *T. nigrescens*, the ethanol/water extract proved to be the richest source of hyperoside (quercetin-3-O-galactoside) and isoquercitrin (42450.94 and 27645.53 mg/kg, respectively). Kaempferol-3-glucoside, rutin and quercetin were also found in high concentrations in this extract (1744.76; 2695.84 and 3830.99 mg/kg, respectively). In addition to the ethanol/water extract, the ethanol extract also showed high concentrations of flavonoids, especially kaempferol-3-glucoside and catechin (2508.80 and 1741.87 mg/kg, respectively). The lowest concentrations of flavonoids were found in the ethyl acetate and water extracts. This result is due to the influence of the polarity of the solvent, as the polarity of ethyl acetate is not conducive to the extraction of flavonoids, while the pronounced polarity of water makes the extraction of flavonoids more difficult due to its chemical structure. In this case, the polarity of the ethanol/water extract is suitable for the efficient extraction of this group of phenolic molecules, which is confirmed by the fact that the total polyphenol content of the plant species *T. nigrescens* was the highest in the ethanol/water extract (111547.70 mg/kg). Only one more study evaluated the phytochemical profile of T. nigrescens prior to this. In that research, the ethyl acetate extract of the aerial parts was subjected to bioassay-guided fractionation, leading to the isolation of a novel biflavone, identified as 4‴,5,5″,7,7″-pentahydroxy-3′,3‴-dimethoxy-3-*O*-β-D-glucosyl-3″,4′-*O*-biflavone, along with eleven known compounds, including three phenolic acids: 4-hydroxy-3,5-dimethylbenzoic acid, p-hydroxybenzoic acid, and p-coumaric acid, and eight flavonoid glycosides (Demirkiran et al., 2013).

Due to the lack of studies, the results of this investigation were also compared with the phytochemical composition of other species of this genus. Thus, when the total phenolic content of the extracts of

T. nigrescens was compared with the total phenolic content of other species (*T. alexandrinum, T. resupinatum, T. hybridum, T. fragiferum, T. incarnatum*), a significantly higher content of total phenols was found in the extracts of T. nigrescens (Kolodziejczyk-Czepas et al., 2014). In addition, the *T. nigrescens* extracts examined in this study were significantly richer in phenolic acids and flavonoids compared to the extracts of *T. pratense* and *T. repens* (Hanganu et al., 2017). Such results are a consequence of the different occurrence of secondary metabolites in plant species of the same genus, but also of the influence of the chosen extraction technique and extraction solvent. Obtaining biologically valuable extracts requires an appropriate selection of procedures and process parameters in order to transfer their use from the laboratory level to the industrial level for the continuous production of end products.

3.3. Antioxidant effects of T. nigrescens extracts

The production of reactive oxygen species under normal physiological conditions is necessary to develop various metabolic processes. However, the constant formation of reactive oxygen species without their removal and accumulation leads to an imbalance between antioxidants and oxidants, resulting in the development of oxidative stress. Oxidative stress causes diseases such as diabetes, cancer, obesity, neurodegenerative diseases, etc. Antioxidants, which can be natural or synthetic, are used to protect the body from oxidative stress. Synthetic antioxidants cause side effects and undesirable effects on health, so natural antioxidants are increasingly being used. Medicinal plants are a rich source of natural antioxidants, which are very attractive for the discovery of potential new medicines due to their diverse structural composition (Njoya, 2021). For all the above reasons, the extracts of *T. nigrescens* were tested for their antioxidant activity (Table 3). The extracts of the aerial parts of *T. nigrescens* were analyzed with different *in vitro* assays based on free radical scavenging mechanism, reduction potential, metal ion chelation, and total antioxidant activity.

The extracts obtained with ethanol and ethanol/water as solvent showed the best ability to scavenge DPPH and ABTS radicals. Indeed, these extracts achieved exceptional activity in scavenging ABTS radicals (88.92 and 88.52 mg TE/g, respectively) and their activity was not statistically significantly different. In the destruction of DPPH radicals, the ethanol/water extract showed the best activity (53.60 mg TE/g). Regarding the reduction potential towards Cu^{2+} and Fe^{3+} ions, the ethanol extract was the most effective (106.90 and 64.77 mg TE/g, respectively). In addition, the ethanol/water extract also showed a significant reduction potential towards Cu^{2+} ions (80.79 mg TE/g). On the other hand, the most effective chelation of metal ions and overall antioxidant activity was achieved by the ethyl acetate extract (14.80 mg EDTAE/g and 1.80 mmol TE/g). This could be the effect of the lower polarity solvent, which extracts less polar components from the plant matrix.

The results obtained indicate that the differences in the antioxidant capacity of the extracts tested can be attributed to how the plant material was prepared and the method used to obtain the extracts. In the study by Kaurinovic et al. (2012), using DPPH, it was confirmed that ethyl acetate and water extracts of *T. pratense* have an antioxidant potential IC_{50} (17.81 and 7.47 μg/mL respectively) and their activity does not differ significantly. In the study conducted by Demirkiran et al. (2013), the ethyl acetate extract of the plant species *T. nigrescens* was found to have antioxidant activity, which was determined using the DPPH test (IC_{50} 12.38 μg/mL). In addition, the antioxidant activity of 70 % ethanol extracts of leaves and flowers of *T. pratense* and *T. repens* was investigated in the study by Hanganu et al. (2017). A stronger antioxidant activity was observed in extracts of the plant species *T. pratense* (IC_{50} 104 μg/mL).

Based on the data available in the literature, it was found that species of the genus *Trifolium* have a pronounced antioxidant capacity. However, numerous studies have investigated extracts obtained with less polar solvents. In contrast, our study investigated the antioxidant potential of extracts obtained with polar solvents, which can be used as natural sources of antioxidants in formulating new products for various industries. On the other hand, the chemical composition of the tested extracts contributed to the activity obtained, which is confirmed by the concentration of phenolic acids and flavonoids identified in the tested extracts. The ethanol/water extract is characterized by the highest concentration of caffeic acid, ferulic acid and ellagic acid, as well as by high concentrations of rutin, isoquercitrin, quercetin and hyperoside, which contribute to a better antioxidant activity of the extract through their synergistic action.

3.4. Enzyme inhibitory effects of T. nigrescens extracts

Since the outbreak of the COVID-19 pandemic, the approach to treatment and nutrition has changed significantly. Research has intensified worldwide and natural ones have replaced synthetic medicines. The reformulation of foods to make greater use of bioactive plant ingredients to increase food safety and reduce sensitivity to allergies has also led to a new concept of functional foods. To define a new concept of functional foods, scientific studies focus on the investigation of underutilized plant species (Lim et al., 2021). Therefore, *T. nigrescens* was investigated for the inhibition of excessive activity of selected enzymes.

As catalysts of biochemical reactions, enzymes are responsible for the development of various metabolic processes in the body. A change in enzyme activity also alters the functioning of the biochemical apparatus and leads to the development of various diseases. The enzyme inhibitory potential of *T. nigrescens* was examined by overactivity of the enzymes AChE, BChE, tyrosinase, α-amylase and α-glucosidase (Table 4).

All the extracts tested showed the ability to inhibit the excessive activity of the AChE enzyme. The inhibitory potency achieved for ethyl acetate, ethanol, and ethanol/water extracts ranged from 2.26 to 2.34 mg GALAE/g and no significant difference was observed between the inhibitory activities of these extracts. In contrast to these extracts, the water extract showed a significantly lower inhibitory activity (0.48 mg GALAE/g) towards the AChE enzyme.

In the inhibition of the BChE enzyme, the ethyl acetate extract was the most potent (4.88 mg GALAE/g), while the ethanol and ethyl/water extracts showed lower activity. The water extract showed no ability to

Table 3
Antioxidant properties[a] of the tested extracts.

Extracts	DPPH (mg TE/g)[b]	ABTS (mg TE/g)[b]	CUPRAC (mg TE/g)[b]	FRAP (mg TE/g)[b]	Chelating (mg EDTAE/g)[c]	PBD (mmol TE/g)[d]
Ethyl acetate	10.37 ± 0.26^{c}	25.93 ± 0.89^{c}	56.93 ± 3.76^{d}	24.35 ± 0.59^{c}	14.80 ± 1.05^{a}	1.80 ± 0.15^{a}
Ethanol	45.76 ± 0.31^{b}	88.92 ± 4.09^{a}	106.90 ± 2.82^{a}	64.77 ± 0.51^{a}	2.93 ± 0.44^{c}	1.40 ± 0.01^{b}
Ethanol/water (70 %)	53.60 ± 1.31^{a}	88.52 ± 2.10^{a}	80.79 ± 1.15^{b}	60.70 ± 2.05^{b}	14.13 ± 0.56^{a}	0.73 ± 0.06^{c}
Water (infused)	47.63 ± 2.41^{b}	79.31 ± 0.27^{b}	68.28 ± 0.68^{c}	61.92 ± 0.47^{v}	7.47 ± 0.41^{b}	0.68 ± 0.03^{d}

[a] values are means ± SD of three measurements. means within each column with different letters (a–d) differ significantly ($p \leq 0.05$)
[b] mg Trolox equivalents per g of extract
[c] mg EDTAE per g of extract
[d] mmol Trolox equivalents per g of extract

Table 4
Enzyme inhibitory properties[a] of the tested extracts.

Extracts	AChE (mg GALAE/g)[b]	BChE (mg GALAE/g)[b]	Tyrosinase (mg KAE/g)[c]	α-amylase (mmol ACAE/g)[d]	α-glucosidase (mmol ACAE/g)[d]
Ethyl acetate	2.26 ± 0.24[a]	4.88 ± 0.45[a]	42.67 ± 0.28[b]	0.71 ± 0.03[a]	0.34 ± 0.01[c]
Ethanol	2.28 ± 0.04[a]	1.61 ± 0.31[c]	47.80 ± 1.96[a]	0.48 ± 0.01[b]	1.11 ± 0.04[a]
Ethanol/water (70 %)	2.34 ± 0.03[a]	2.34 ± 0.27[b]	48.97 ± 0.31[a]	0.31 ± 0.01[c]	1.01 ± 0.16[b]
Water (infused)	0.48 ± 0.03[b]	na	2.61 ± 0.54[c]	0.06 ± 0.01[d]	0.23 ± 0.01[d]

na – not active
[a] values are means ± SD of three measurements, means within each column with different letters (a–d) differ significantly ($p \leq 0.05$)
[b] mg Galantamine equivalents per g of extract
[c] mg Kojic acid per g of extract
[d] mmol Acarbose equivalents per g of extract

inhibit the excessive activity of the BChE enzyme. The results shown are due to the influence of the extraction technique and the solvent used to obtain the extracts. Indeed, in the inhibition of enzymes whose excessive activity is associated with the development of neurological diseases, it was observed that the extract with lower polarity obtained a better inhibition potential, which could be a consequence of the influence of less polar molecules extracted with this solvent.

Tyrosinase is an enzyme whose excessive activity can lead to the appearance of hyperpigmentation of the skin. If the work of this enzyme is not controlled, it can lead not only to hyperpigmentation but also to the appearance of melanoma. Synthetic drugs are still used in therapy. In order to reduce their use, extracts of *T. nigrescens* have been investigated as potential natural tyrosinase inhibitors. In reducing tyrosinase activity, the best inhibitory potential was achieved by ethanol and ethanol/water extracts (47.80 and 48.97 mg KAE/g, respectively), whose activity was not statistically significantly different. The ethyl acetate extract also showed a good inhibitory effect (42.67 mg KAE/g), while the water extract showed the weakest effect (2.61 mg KAE/g). The achieved inhibitory power indicates that ethanol or ethanol/water is the best and most efficient method to extract polar molecules from plant material. Mixing ethanol and water changes the dielectric constant and it is possible to extract less polar compounds. On the other hand, water as a solvent extracts highly polar compounds due to its dielectric constant, which influences the achieved biological activity.

In addition to proper digestion, the work of the enzymes of the digestive system is also very important for protecting the body against diseases such as diabetes. Excessive activity of the enzymes α-amylase and α-glucosidase leads to an increase in blood sugar levels, which is why various medications are used to prevent this disease. To protect their health, patients are increasingly turning to herbal medicines. Therefore, extracts of *T. nigrescens* have been tested for their inhibition of excessive α-amylase and α-glucosidase activity. The results of the study show that the extracts obtained with less polar solvents inhibit the enzymes α-amylase and α-glucosidase more effectively. As far as the inhibition of α-amylase is concerned, the ethyl acetate extract achieved the best inhibitory effect (0.71 mmol ACAE/g), while the most effective inhibition of α-glucosidase was achieved by the ethanol extract (1.11 mmol ACAE/g). Using HPLC analysis, the ethanol extract was found to be a very rich source of gallic acid, catechin, kaempferol-3-glucoside, kaempferol, and isorhamnetin, thus it is hypothesized that these secondary metabolites, identified in high concentrations in the ethanol extract, contributed to the antidiabetic activity realized. To our knowledge, there is only one study that reports on the inhibitory properties of the ethyl acetate extract of the leaves of the plant species *T. nigrescens* on the enzyme tyrosinase (Demirkiran et al., 2013). In this study, the flavonoid glycosides showed exceptional potential to inhibit the excessive tyrosinase enzyme activity, more so than kojic acid as a synthetic inhibitor. These results suggest that the selected plant species is very important for further research, which could be based on the optimization of the extraction process to extract potent secondary metabolites more efficiently.

3.5. Anti-biofilm activity of *T. nigrescens* extracts

Based on the results of the minimum inhibitory concentration (MIC, Table 5), we used two concentrations, 10 μg/mL and 20 μg/mL, to evaluate the putative ability of the extracts to inhibit the mature biofilm of the bacteria (by the crystal violet test) and the metabolism of their sessile cells (by the MTT test). The results are shown in Table 6.

The extracts showed activity against the five pathogenic strains tested in most cases and at their highest concentration, except *L. monocytogenes*, which showed no sensitivity to the ethanol extract. In contrast, *P. aeruginosa* resisted all four extracts, with inhibitory activity not exceeding 3.03 %. The ethyl acetate extract, except P. *aeruginosa*, was effective against the biofilm of the pathogenic strains, achieving inhibition rates of up to 57.21 % against *L. monocytogenes* and no less than 13.51 % against *A. baumannii*.

The ethanol/water extract showed stronger activity against *A. baumannii* (27.41 %) but was less effective against *L. monocytogenes* than the ethyl acetate extract, although it still achieved 28.81 % inhibition against this pathogen. A notable observation is the contrasting behavior of the extracts against *A. baumannii* and *L. monocytogenes*. For *A. baumannii*, the inhibitory effect of the extracts increased in the following order: ethyl acetate (13.51 %) → ethanol (21.70 %) → ethanol/water (27.94 %) → water (34.94 %). This trend indicates that the higher water content in the extraction process positively influences the inhibitory activity of the extracts. In contrast, for *L. monocytogenes*, using water or ethanol alone in the extraction process resulted in lower efficacy. The water extract showed no activity, while the ethanol/water mixture inhibited the mature biofilm by 28.81 %. However, the ethyl acetate extract was the most effective, achieving 57.21 % inhibition of mature biofilm. To our knowledge, this is the first time that the potential biofilm activity of *T. nigrescens* has been determined. Other *Trifolium* species (*T. alexandrinum*, *T. incarnatum*, *T. resupinarum* var. *resupinarum*) were shown to be capable of inhibiting *Candida albicans* and to a lesser extent *Candida glabrata* (Budzyńska et al., 2014). Cankaya and Somuncuoglu (2021) reported the presence of numerous secondary metabolites, especially saponins and flavonoids, in the genus *Trifolium*, including *T. resupinarum*, *T. alexandrinum*, *T. incarnatum*, with biological properties, including blocking some enzymatic activities of pathogens involved in respiratory diseases and an effect against *C. albicans*.

In contrast, Ngangom et al. (2023) demonstrated the efficacy of bioactive compounds from *T. repens* against 22 pathogenic proteins involved in biofilm formation, in particular *S. aureus*, *P. aeruginosa* and *A. baumannii*. The authors hypothesised that the antibacterial effect of *T. repens* was mainly due to the presence of naringenin and tripholin, which were not found in the four extracts of *T. nigrescens*. Khan et al. (2012) investigated the antibacterial activity of extracts from the leaves of *T. alexandrinum* and found a certain effect against *S. aureus*, *P. aeruginosa* and *E. coli*. The four extracts showed different behavior when we analysed their potential inhibitory activity against the metabolism of the sessile cells of the mature biofilm. The test performed with MTT showed that none of the extracts was able to inhibit the metabolism of the sessile cells of *A. baumanni* and *E. coli*. Only the water extract showed a minimal

Table 5
Minimal inhibitory concentration of the extracts (μg/mL).

MIC	*AB*	*EC*	*LM*	*PA*	*SA*
EA	38.0 ± 2.0^{a}	$> 50^{b}$	$> 50^{b}$	$> 50^{b}$	46.0 ± 1.0^{a}
EtOH	$> 50^{b}$	$> 50^{b}$	$> 46 \pm 2.0^{b}$	$> 50^{b}$	46.0 ± 1.0^{a}
EtOH/Water	40.0 ± 3.0^{a}	$> 50^{b}$	$> 50^{b}$	$> 50^{b}$	$> 50^{b}$
Water	36.0 ± 2.0^{a}	$> 50^{b}$	$> 50^{b}$	$> 50^{b}$	$> 50^{b}$
C	31.0 ± 1.0	31.0 ± 2.0	30.0 ± 1.0	28.0 ± 1.0	32.0 ± 1.0

AB = A. baumannii; EC = E. coli; LM = L. monocytogenes; PA = P. aeruginosa; SA = S. aureus. As control (C), we used tetracycline.
[1] values are means ± SD of three measurements, means within each column with different letters (a–b) differ significantly ($p \leq 0.05$).

Table 6
Percentage of inhibition[a] compared to the control (untreated bacteria) for whose the inhibition was assumed as = 0.

CV	EA-10 μg/mL	EA- 20 μg/mL	EtOH- 10 μg/mL	EtOH-20 μg/mL	EtOH/Water- 10 μg/mL	EtOH/Water-20 μg/mL	Water- 10 μg/mL	Water- 20 μg/mL
AB	1.29^{ns} (±0.02)	13.51^{a} (±0.44)	0.00 (±0.00)	21.70^{a} (±1.14)	20.98^{a} (±1.12)	27.84^{b} (±1.67)	29.64^{b} (±2.08)	34.94^{b} (±3.12)
EC	0.00 (±0.00)	14.25^{a} (±0.62)	2.39^{ns} (±1.03)	18.71^{a} (±0.87)	0.00 (±0.00)	17.12^{a} (±1.15)	0.00 (±0.00)	6.54^{a} (±0.87)
LM	17.41^{a} (±1.22)	57.21^{c} (±1.77)	0.00 (±0.00)	0.00 (±0.00)	2.63^{ns} (±2.01)	28.81^{b} (±1.86)	0.00 (±0.00)	0.00 (±0.00)
PA	0.00 (±0.00)	0.00 (±0.00)	0.00 (±0.00)	0.28^{ns} (±0.11)	0.00 (±0.00)	0.00 (±0.00)	0.00 (±0.00)	3.03^{ns} (±0.31)
SA	0.00 (±0.00)	23.24^{a} (±2.02)	0.00 (±0.00)	29.38^{b} (±2.41)	0.00 (±0.00)	12.12^{a} (±0.43)	0.00 (±0.00)	17.62^{a} (±1.55)
MTT	**EA−10 μg/mL**	**EA- 20 μg/mL**	**EtOH- 10 μg/mL**	**EtOH−20 μg/mL**	**EtOH/Water- 10 μg/mL**	**EtOH/Water−20 μg/mL**	**Water- 10 μg/mL**	**Water- 20 μg/mL**
AB	0.00 (±0.00)	0.00 (±0.00)	0.00 (±0.00)	0.00 (±0.00)	0.00 (±0.00)	0.00 (±0.00)	0.00 (±0.00)	4.25^{a} (±0.12)
EC	0.00 (±0.00)	0.00 (±0.00)	0.00 (±0.00)	10.54^{a} (±0.85)	0.00 (±0.00)	0.00 (±0.00)	0.00 (±0.00)	0.00 (±0.00)
LM	0.00 (±0.00)	0.00 (±0.00)	0.00 (±0.00)	18.95^{a} (±1.27)	0.00 (±0.00)	0.00 (±0.00)	0.00 (±0.00)	42.92^{b} (±3.13)
PA	7.24^{a} (±0.26)	11.65^{a} (±1.09)	0.00 (±0.00)	46.98^{b} (±2.67)	0.00 (±0.00)	49.53^{c} (±2.98)	13.94^{a} (±1.19)	33.72^{b} (±2.76)
SA	15.48^{a} (±1.03)	16.13^{a} (±0.86)	45.85^{b} (±2.23)	47.85^{b} (±1.54)	41.69^{b} (±1.67)	47.15^{b} (±1.22)	30.46^{b} (±2.57)	57.38^{c} (±4.02)

CV: inhibitory activity of extracts in the crystal violet assay.
The experiments were performed on mature biofilm, that is the extracts were added after 24 h of bacterial biofilm formation.
[a] values are means ± SD of three measurements, means within each column with different letters (a–d) differ significantly ($p \leq 0.05$)

inhibitory effect (4.25 %) against *A. baumannii* at the highest concentration used. *L. monocytogenes*, which had also proved to be sensitive to the effect of the extracts, showed an inhibitory effect on its sessile cells in the MTT test after the addition of only the ethanolic extract (inhibition = 18.85 %) and especially the water extract, whose presence caused an inhibition of 42.92 %. In contrast to what we observed in the crystal violet test, the extracts inhibited the metabolism of the sessile cells of *P. aeruginosa* with an inhibition level between 7.24 % and 49.53 %. Even more drastic was the effect of the extracts on the metabolism of the sessile cells of *S. aureus*. In this case, we observed an inhibitory effect that reached 45.5 % inhibition already at 10 μg/mL of the extract in ethanol/water and a higher value (57.38 %) when the strain was incubated with 20 μg/mL. Therefore, we must agree with the hypothesis supported by other studies, such as that of Nazzaro et al. (2024), who found that the extracts that act on the biofilm do not always inhibit the metabolic pathway.

In the correlation analysis performed considering the most abundant polyphenols in all four extracts and the efficacy of the extracts on the pathogens, we found that isoquercitrin and delphinidin 3,5-diglucoside ($\rho = 0.86$), caffeic acid ($\rho = 0.84$), *p*-coumaric acid ($\rho = 0.83$) and rutin (ρ=0.72) appeared to be the polyphenols most strongly associated with the potential inhibitory effect of the four extracts on the mature biofilm of *A. baumannii*. Rutin has antibiofilm activity against *A. baumannii*, which has been demonstrated by Pourhajibagher et al. (2024).

The results of the MTT assay confirmed the influence of *p*-coumaric acid on the metabolism of sessile cells of *A. baumannii*. However, other polyphenols showed much lower correlation values (e.g. rutin showed a very low correlation, $\rho = 0.10$) or their correlation values almost halved (e.g. gallic acid decreased from $\rho = 0.79$ to $\rho = 0.41$ when we compared the inhibition values from the CV and MTT assays). A negative correlation was observed between the concentration of 3-hydroxybenzoic acid and the inhibitory effect of the extracts on the mature biofilm and sessile cell metabolism of *A. baumannii*, with correlation values of $\rho = -0.96$ and $\rho = -0.58$, respectively. While the extracts showed an inhibitory effect on the biofilm, their influence on sessile cell metabolism was probably impaired by the 3-hydroxybenzoic acid. This negative effect was possibly partially attenuated by the positive influence of other polyphenols such as caffeic acid, rutin, *p*-coumaric acid, isoquercitrin and delphinidin 3,5-diglucoside. However, these compounds were not sufficient to completely counteract the effect of 3-hydroxybenzoic acid. In particular, *p*-coumaric acid alone ($\rho = 0.84$) could not compensate for the limited influence of the other polyphenols, some of which showed negative or even lower correlation values than those obtained when comparing the polyphenol concentrations with the percentages of biofilm inhibition in the MTT assay. In the case of *E. coli*, the inhibitory effect of the extracts on biofilm appeared to be primarily influenced by kaempferol and kaempferol-3-glucoside ($\rho = 0.73$ and 0.74, respectively) and ferulic acid ($\rho = 0.56$). However, *p*-coumaric acid ($\rho = -0.83$) harmed the efficacy of the extracts, in contrast to its role in *A. baumannii*.

The extracts showed little or no inhibitory effect on the metabolism of sessile cells of *E. coli*. Neither catechin ($\rho = 0.98$) nor kaempferol-3-glucoside ($\rho = 0.87$) and kaempferol ($\rho = 0.79$) were sufficient to overcome the negative influence of hyperoside ($\rho = -0.77$), *p*-coumaric

acid (ρ = −0.67), caffeic acid (ρ = −0.55) and ferulic acid (ρ = −0.58).

For *L. monocytogenes*, the ethyl acetate and ethanol/water extracts showed significant inhibition of biofilm in the crystal violet assay, while the ethanolic and water extracts were most effective against sessile cell metabolism. The correlation analysis indicates that 3-hydroxybenzoic acid (ρ = 0.79) has a positive influence on biofilm inhibition and counteracts the negative influence of other polyphenols such as gallic acid (ρ = −0.94). Ellagic acid, quercitrin and kaempferol negatively influenced the performance of the extracts in biofilm formation, while gallic acid (ρ = 0.63) and *p*-coumaric acid (ρ = 0.57) were more relevant for the inhibition of sessile cell metabolism.

In *P. aeruginosa*, which was generally resistant to the extracts, *p*-coumaric acid (ρ = 0.80) could not counterbalance the negative effects of 3-hydroxybenzoic acid and catechin (ρ = −0.60). However, the extracts inhibited the metabolism of sessile cells, influenced by rutin (ρ = 0.90), gallic acid (ρ = 0.85), kaempferol, kaempferol-3-glucoside (ρ = 0.84 and 0.67, respectively), quercetin ρ = 0.82) and delphinidin-3,5-diglucoside (ρ = 0.67). It is noteworthy that all polyphenols except 3-hydroxybenzoic acid showed positive correlation values.

In the case of *S. aureus*, the effect of the extracts on biofilm formation correlated with the presence of catechin (ρ = 0.75), 3-hydroxybenzoic acid (ρ = 0.47), and kaempferol-3-glucoside (ρ = 0.42). In the inhibition of sessile cell metabolism, the most important polyphenols were gallic acid (ρ = 0.90), rutin (ρ = 0.78), isoquercitrin and delphinidin-3,5-diglucoside (for both ρ was = 0.76). This confirms the positive correlation between anti-biofilm activity and the presence of delphinidin 3,5-diglucoside and anthocyanins (Pejin et al., 2017; Zhang et al., 2020). Therefore, we have confirmed the different influence of some secondary metabolites on the inhibitory effect of natural extracts in other cases (Salem et al., 2022; Zengin et al., 2024).

3.6. Molecular docking

Molecular docking simulations were conducted using hub molecules derived from *T. nigrescens* to assess their binding affinities toward a range of bacterial and fungal target proteins. The ligands evaluated during the docking analyses included rutin, kaempferol-3-O-glucoside, catechin, quercetin, kaempferol, isorhamnetin, isoquercitrin, delphindin-3-galactoside, and 4-hydroxy benzoic acid, Ferulic acid, p-coumaric acid, hyperoside, 3-Hydroxy benzoic acid, ellagic acid, caffeic acid, delphinidin-3–5-diglucoside, and phloridzin. These were tested against key proteins *from A. baumannii, L. monocytogenes,* and *S. aureus*, as well as standard enzymes (AChE, BChE, glucosidase, amylase, and tyrosinase). Among the complexes investigated, Isoorientin demonstrated the highest binding affinity in complexes with Isoquercitrin-BChE (-10.6 kcal/mol), hyperoside-BChE (-10.5 kcal/mol), and kaempferol-3-O-glucoside-BChE, thereby achieving the most favorable binding scores. RMSD values ranged from 0.01 to 8.4, reflecting both structural stability and flexibility in the docked complexes. Given the critical role that RMSD plays in evaluating the stability and reliability of docking poses, the compounds selected for further analysis were required to meet the following criteria: a binding affinity of −9 kcal/mol or lower, an RMSD value of 2 Å or below, and the formation of at least four hydrogen bond (Hbond) (Table 7 and Fig. 1A).

AChE analyses indicated a strong potential for enzyme inhibition, with catechin (8 Hbond, −9.6 kcal/mol), quercetin (9 Hbond, −9.7 kcal/mol), kaempferol (4 Hbond, −9.8 kcal/mol), and isorhamnetin (6 Hbond, −9.5 kcal/mol), delphindin-3-galactoside (9 Hbond, −9.2 kcal/mol), and Ellagic acid (7 Hbond, −10.3 kcal/mol) all demonstrated notable interactions. Of particular interest is the observation that ellagic acid exhibited a highly negative binding energy of −10.3 kcal/mol and interacted with ASP A:74, GLY A:120, TYR A:124, TYR A:133, TYR A:341, and HIS A:447. The identification of hotspot residues, such as ASP A:74, GLY A:120, TYR A:133, TYR A:337, and HIS A:447, suggests that AChE contains potentially critical binding pockets.

In the context of BChE, the following compounds were evaluated: Kaempferol-3-O-glucoside (10 Hbond, −10.4 kcal/mol), isoquercitrin (11 Hbond, −10.6 kcal/mol), delphindin-3 -galactoside (10 Hbond, −9.9 kcal/mol), hyperoside (9 Hbond, −10.5 kcal/mol), and phloridzin (5 Hbond, −9.5 kcal/mol). These ligands were frequently found to interact with ASP A:70, GLY A:115, TYR A:128, SER A:198, and TYR A:332, with isoquercitrin (-10.6 kcal/mol) exhibiting the strongest interaction profile.

A docking analysis was performed for amylase, which exhibited an average of 6.50 Hbond and a binding energy of −9.60 kcal/mol. This analysis identified rutin, which formed 8 Hbond and exhibited a binding energy of −10.1 kcal/mol, and quercetin, which formed 5 Hbond and exhibited a binding energy of −9.1 kcal/mol, as the most significant ligands. Rutin formed stable interactions with GLN A:63, ARG A:195, LYS A:200, GLU A:233, ILE A:235, HIS A:299, and HIS A:305, providing a notably negative binding energy of −10.1 kcal/mol.

Within *Acinetobacter baumannii*, the Beta-lactamase target (10 Hbond, −9.1 kcal/mol) was effectively inhibited by Hyperoside (10 Hbond, −9.1 kcal/mol), which interacted with SER A:80, GLU A:113, LYS A:125, SER A:127, SER A:218, and TRP A:220. Against EPSP synthase (10 Hbond, −9.7 kcal/mol), Rutin bound SER A:335, ARG A:339, GLN A:483, ARG A:508, LYS A:657, SER A:659, ARG A:661, and ASP A:708. GlmU (8 Hbond, −9.4 kcal/mol) also showed strong interactions with rutin, which targeted LYS A:22, GLN A:73, GLY A:78, THR A:79, ASP A:102, VAL A:220, GLY A:222, and ASN A:224. In the OXA-231 target (9.38 Hbond, −9.39 kcal/mol), rutin, kaempferol-3-O-glucoside, quercetin, kaempferol, isorhamnetin, hyperoside, ellagic acid, and delphinidin-3–5-diglucoside all presented high hydrogen bond counts and low RMSD values, frequently binding SER A:81, SER A:128, SER A:219, TRP A:221, and ARG A:261.

In the *Listeria monocytogenes*, the InlA target demonstrated strong inhibition when exposed to isoquercitrin, delphindin-3-galactoside, hyperoside, and delphinidin-3–5-diglucoside. These compounds exhibited elevated hydrogen bond formation and sufficiently negative binding energies. Key residues included LYS A:425, SER A:429, THR A:454, ASP A:457, and THR A:459. Within the same organism, MurA1 interacted notably with rutin (11 Hbond, −9.6 kcal/mol), delphindin-3-galactoside (-9.2 kcal/mol), and delphinidin-3–5-diglucoside (13 Hbond, −9.6 kcal/mol), binding to ASN A:23, SER A:163, and VAL A:164. These results suggest that a low RMSD, high hydrogen bond count, and binding energies of −9 kcal/mol or lower are critical for potent inhibition of InlA and MurA1.

In the *Staphylococcus aureus*, MurE was targeted by kaempferol-3-O-glucoside, catechin, quercetin, kaempferol, isoquercitrin, and delphindin-3-galactoside, and ellagic acid, all of which repeatedly interacted with LYS A:114, THR A:152, ASP A:204, HIS A:205, and ARG A:383. Catechin (13 Hbond, −10.1 kcal/mol) demonstrated particularly robust binding, while quercetin (11 Hbond, −9.5 kcal/mol) and kaempferol-3-O-glucoside (13 Hbond, −9.1 kcal/mol) also exhibited stable binding. In the PBP4 (13 Hbond, −9.40 kcal/mol) of the same organism, rutin formed 13 Hbond with SER A:75, GLU A:114, ASN A.:138, SER A:139, GLY A:181, GLU A:183, THR A:260, GLY A:261, and SER A:262.

The findings of this study indicate that for bacterial target proteins *A. baumannii, L. monocytogenes,* and *S. aureus* and standard enzymes, an RMSD of 2 Å or less, a minimum of four Hbond, and binding energies of approximately −9 kcal/mol or more negative generally indicate stable and potent binding interactions. The observation that specific amino acid residues are frequently targeted emphasizes their potential as critical binding pockets for inhibitor design. Consequently, the findings confirm that low RMSD, high hydrogen bond formation, and significantly negative binding energies are key parameters in predicting the inhibitory potential of these compounds.

3.7. Molecular dynamics simulation

In this study, molecular dynamics (MD) simulations were conducted

Table 7
The docking score (kcal/mol) and interacting residues of the enzyme and protein.

Compound	Target	PDB ID	Binding energy	RMSD	Interaction		Binding site
					Type	Number	
Rutin	*Amylase*	2QV4	−10.1	0.7	Hbond	8	GLN A:63;ARG A:195;ARG A:195;LYS A:200;GLU A:233;ILE A:235; HIS A:299;HIS A:305
Quercetin	*Amylase*	2QV4	−9.1	0.37	Hbond	5	GLN A:63;ARG A:195;ARG A:195;ASP A:197;HIS A:299
Catechin	*AChE*	7E3H	−9.6	1.07	Hbond	8	TYR A:72;ASP A:74;ASN A:87;GLY A:120;GLY A:120;TYR A:133; TYR A:337;TYR A:337
Quercetin	*AChE*	7E3H	−9.7	0.69	Hbond	9	ASP A:74;ASP A:74;TRP A:86;ASN A:87;GLY A:120;TYR A:133;TYR A:133;TYR A:337;HIS A:447
Kaempferol	*AChE*	7E3H	−9.8	0.37	Hbond	4	ASP A:74;GLY A:120;TYR A:124;TYR A:133
Isorhamnetin	*AChE*	7E3H	−9.5	0.32	Hbond	6	ASP A:74;GLY A:120;TYR A:124;SER A:125;GLU A:202;TYR A:337
Delphindin−3-galactoside	*AChE*	7E3H	−9.2	0.82	Hbond	9	TYR A:72;ASP A:74;ASP A:74;GLY A:121;GLY A:126;GLU A:202; GLU A:202;PHE A:295;HIS A:447
Ellagic acid	*AChE*	7E3H	−10.3	0.92	Hbond	7	ASP A:74;GLY A:120;TYR A:124;TYR A:133;TYR A:133;TYR A:341; HIS A:447
Kaempferol−3-O-glucoside	*BChE*	6EQP	−10.4	1.08	Hbond	10	ASP A:70;GLY A:78;TRP A:82;GLY A:115;TYR A:128;TYR A:128; GLU A:197;SER A:198;SER A:198;LEU A:286
Isoquercitrin	*BChE*	6EQP	−10.6	0.57	Hbond	11	ASP A:70;SER A:79;TRP A:82;GLY A:115;GLY A:115;TYR A:128; TYR A:128;SER A:198;PRO A:285;TYR A:332;HIS A:438
Delphindi- 3-galactoside	*BChE*	6EQP	−9.9	1.01	Hbond	10	ASP A:70;SER A:79;GLY A:115;GLY A:117;THR A:120;TYR A:128; GLU A:197;SER A:198;LEU A:286;TYR A:332
Hyperoside	*BChE*	6EQP	−10.5	0.16	Hbond	9	ASP A:70;ASP A:70;GLY A:115;GLY A:116;GLY A:117;TYR A:128; TYR A:128;SER A:198;SER A:198
Ellagic acid	*BChE*	6EQP	−10.0	7.3	Hbond	5	ASP A:70;GLY A:115;TYR A:128;GLU A:197;TYR A:332
Phloridzin	*BChE*	6EQP	−9.5	0.45	Hbond	5	ASP A:70;ASP A:70;ASN A:83;TYR A:128;TYR A:332
Rutin	*S. aureus_MurE*	4C13	−11.3	6.6	Hbond	17	LYS A:114;THR A:115;THR A:115;THR A:115;THR A:152;ASP A:204;ASP A:204;HIS A:205;HIS A:205;HIS A:205;ASP A:207;ARG A:335;ARG A:335;TYR A:351;ARG A:383;ASN A:407;GLU A:460
Kaempferol−3-O-glucoside	*S. aureus_MurE*	4C13	−9.1	0.3	Hbond	13	LYS A:114;THR A:152;THR A:152;ASP A:204;ASP A:204;HIS A:205;HIS A:205;HIS A:205;TYR A:351;TYR A:351;ARG A:383; ARG A:383;SER A:456
Catechin	*S. aureus_MurE*	4C13	−10.1	0.1	Hbond	13	THR A:111;GLY A:113;GLY A:113;LYS A:114;LYS A:114;THR A:115;THR A:115;THR A:115;SER A:116;SER A:116;SER A:116; ASN A:301;ARG A:335
Quercetin	*S. aureus_MurE*	4C13	−9.5	1.0	Hbond	11	GLY A:113;LYS A:114;LYS A:114;THR A:115;THR A:115;SER A:116;ASP A:204;HIS A:205;ARG A:335;HIS A:353;GLY A:357
Kaempferol	*S. aureus_MurE*	4C13	−9.1	0.8	Hbond	6	LYS A:114;THR A:115;SER A:116;SER A:116;THR A:152;ASN A:301
Isorhamnetin	*S. aureus_MurE*	4C13	−9.6	8.4	Hbond	9	GLY A:113;LYS A:114;THR A:115;THR A:115;SER A:116;GLU A:177;ASN A:301;ARG A:335;GLY A:357
Isoquercitrin	*S. aureus_MurE*	4C13	−9.6	0.7	Hbond	12	LYS A:114;THR A:152;THR A:152;ASP A:204;ASP A:204;HIS A:205;HIS A:205;HIS A:353;ARG A:383;ARG A:383;ASN A:407; GLU A:460
Delphindin−3-galactoside	*S. aureus_MurE*	4C13	−9.3	0.4	Hbond	16	LYS A:114;THR A:115;THR A:137;ALA A:150;ALA A:150;ASN A:151;THR A:152;THR A:152;THR A:153;SER A:179;ARG A:187; ARG A:187;HIS A:205;TYR A:351;ARG A:383;ARG A:383
Hyperoside	*S. aureus_MurE*	4C13	−9.3	nd	Hbond	12	LYS A:114;THR A:152;THR A:152;ASP A:204;ASP A:204;HIS A:205;HIS A:205;ASP A:207;ARG A:383;ASN A:407;SER A:456; GLU A:460
Ellagic acid	*S. aureus_MurE*	4C13	−9.1	1.1	Hbond	7	GLY A:113;LYS A:114;LYS A:114;THR A:115;THR A:115;SER A:116;HIS A:353
Rutin	*S. aureus_PBP4*	5TW8	−9.4	0.0	Hbond	13	SER A:75;SER A:75;SER A:75;GLU A:114;GLU A:114;ASN A:138; SER A:139;GLY A:181;GLU A:183;GLU A:183;THR A:260;GLY A:261;SER A:262
Rutin	*L. monocytogenes_InlA*	1O6T	−9.4	6.5	Hbond	12	LYS A:425;LYS A:425;SER A:429;SER A:429;SER A:429;SER A:429; SER A:429;THR A:454;THR A:454;ASP A:457;ASP A:457;ASP A:457
Isoquercitrin	*L. monocytogenes_InlA*	1O6T	−9.1	0.3	Hbond	16	LYS A:425;LYS A:425;SER A:429;SER A:429;SER A:429;SER A:429; SER A:429;SER A:429;SER A:429;THR A:454;ASP A:457;ASP A:457;ASP A:457;ASP A:457;THR A:459;THR A:459
Delphindin−3-galactoside	*L. monocytogenes_InlA*	1O6T	−9.1	0.3	Hbond	15	LYS A:425;LYS A:425;LYS A:425;SER A:429;SER A:429;SER A:429; SER A:429;SER A:429;SER A:429;THR A:454;THR A:454;ASP A:457;ASP A:457;ASP A:457;THR A:459
Hyperoside	*L. monocytogenes_InlA*	1O6T	−9.2	0.6	Hbond	14	LYS A:425;LYS A:425;SER A:429;SER A:429;SER A:429;SER A:429; SER A:429;THR A:454;GLU A:455;ASP A:457;ASP A:457;ASP A:457;THR A:459;THR A:459
Delphinidin−3−5-diglucoside	*L. monocytogenes_InlA*	1O6T	−9.8	0.6	Hbond	18	ASN A:423;LYS A:425;LYS A:425;LYS A:425;LYS A:425;ASN A:427; VAL A:428;SER A:429;SER A:429;SER A:429;SER A:429;SER A:429; SER A:429;SER A:429;SER A:429;THR A:454;ASP A:457;THR A:459
Rutin	*L. monocytogenes_MurA1*	3R38	−9.6	0.1	Hbond	11	ASN A:23;GLY A:120;SER A:163;SER A:163;SER A:163;VAL A:164; GLN A:168;ARG A:233;ASP A:305;ARG A:331;ARG A:331
Delphindin−3-galactoside	*L. monocytogenes_MurA1*	3R38	−9.2	1.1	Hbond	11	ASN A:23;ASN A:23;ARG A:122;ARG A:122;HIS A:127;SER A:163; VAL A:164;GLY A:165;ALA A:166;GLU A:189;ARG A:331

(*continued on next page*)

Table 7 (*continued*)

Compound	Target	PDB ID	Binding energy	RMSD	Interaction		Binding site
					Type	Number	
Delphinidin−3–5-diglucoside	*L. monocytogenes_MurA1*	3R38	−9.6	0.5	Hbond	13	ASN A:23;ASN A:23;PRO A:123;HIS A:127;SER A:163;VAL A:164; GLN A:168;GLU A:189;GLU A:191;ARG A:233;ARG A:233;THR A:304;ASP A:305
Kaempferol	*L. monocytogenes_PrfA*	6EXL	−9.1	1.1	Hbond	3	LYS A:64;LYS A:64;GLN A:146
Rutin	*A. baumannii_OXA−231*	6NZ8	−9.5	0.2	Hbond	12	SER A:81;MET A:125;MET A:125;SER A:128;LYS A:218;SER A:219; SER A:219;TRP A:221;TRP A:221;ARG A:261;ASN A:262;TYR A:266
Kaempferol−3-O-glucoside	*A. baumannii_OXA−231*	6NZ8	−9.2	1.1	Hbond	9	SER A:81;SER A:128;SER A:128;SER A:128;SER A:128;TRP A:221; TRP A:221;ARG A:261;ARG A:261
Quercetin	*A. baumannii_OXA−231*	6NZ8	−9.6	1.1	Hbond	10	SER A:81;SER A:81;SER A:81;SER A:128;SER A:128;TRP A:221; MET A:223;MET A:223;ARG A:261;ARG A:261
Kaempferol	*A. baumannii_OXA−231*	6NZ8	−9.4	0.0	Hbond	8	SER A:81;SER A:81;SER A:128;SER A:128;TRP A:221;TRP A:221; ARG A:261;ARG A:261
Isorhamnetin	*A. baumannii_OXA−231*	6NZ8	−9.8	1.1	Hbond	11	SER A:81;SER A:81;SER A:128;SER A:128;TRP A:221;TRP A:221; MET A:223;MET A:223;ALA A:224;ARG A:261;ARG A:261
Hyperoside	*A. baumannii_OXA−231*	6NZ8	−9.1	0.1	Hbond	6	SER A:128;SER A:128;SER A:219;TRP A:221;ARG A:261;ARG A:261
Ellagic acid	*A. baumannii_OXA−231*	6NZ8	−9.3	0.9	Hbond	7	SER A:81;SER A:128;SER A:219;SER A:219;TRP A:221;ARG A:261; ARG A:261
Delphinidin−3–5-diglucoside	*A. baumannii_OXA−231*	6NZ8	−9.2	1.6	Hbond	12	TYR A:112;MET A:125;ALA A:126;SER A:128;LYS A:218;SER A:219;SER A:219;SER A:219;TRP A:221;ARG A:261;ASN A:262; ASN A:262
Rutin	*A. baumannii_GlmU*	5VMK	−9.4	1.1	Hbond	8	LYS A:22;GLN A:73;GLY A:78;THR A:79;ASP A:102;VAL A:220; GLY A:222;ASN A:224
Rutin	*A. baumannii_Beta lactamase*	5L2F	−9.1	nd	Hbond	12	SER A:80;SER A:80;GLU A:113;GLU A:113;LYS A:125;SER A:127; SER A:218;TRP A:220;TRP A:220;TRP A:220;TRP A:222;SER A:257
Hyperoside	*A. baumannii_Beta lactamase*	5L2F	−9.1	0.1	Hbond	10	SER A:80;SER A:80;SER A:80;GLU A:113;LYS A:125;SER A:127; SER A:218;SER A:218;TRP A:220;TRP A:220
Rutin	*A. baumannii_EPSP Synthase*	5BUF	−9.7	0.1	Hbond	10	SER A:335;SER A:335;ARG A:339;ARG A:339;GLN A:483;ARG A:508;LYS A:657;SER A:659;ARG A:661;ASP A:708

[1]values of nd means: not determined.

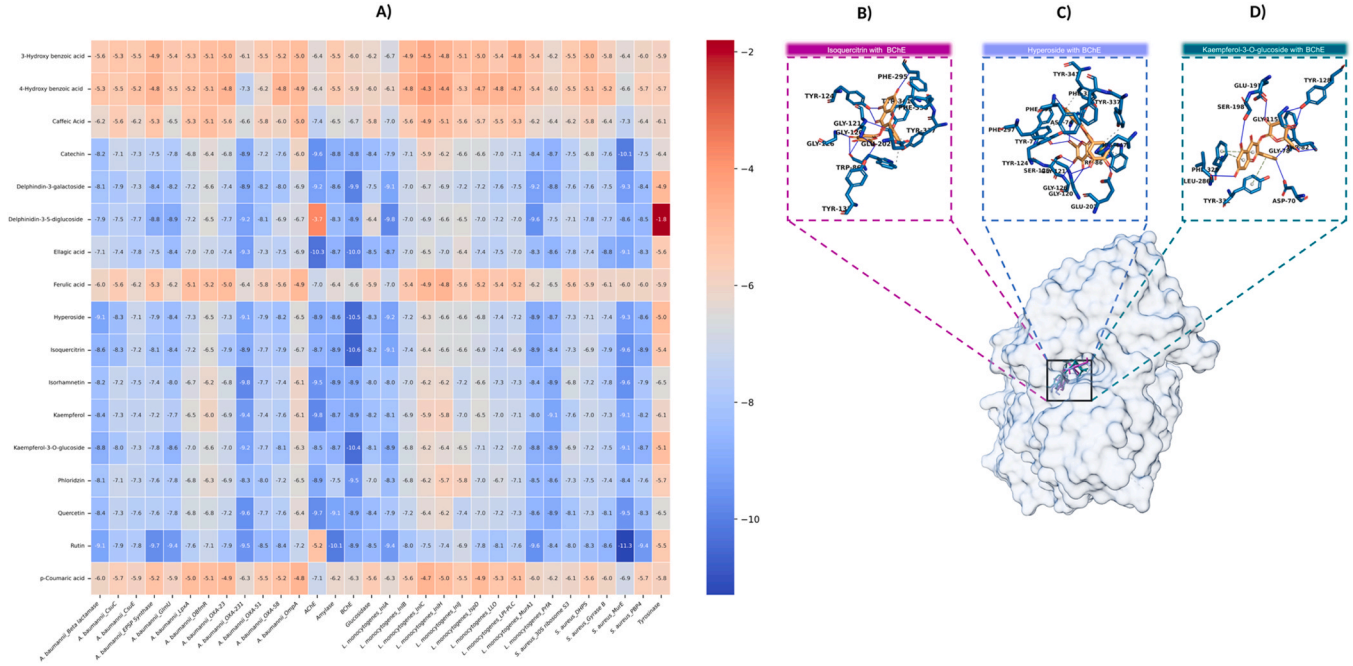

Fig. 1. A comprehensive analysis of the binding interactions between enzymes/proteins and the selected compounds: A) A graphical representation of docking scores for relevant enzymes/proteins. B) Molecular interaction analysis of Isoquercitrin with *BChE*. C) Molecular interaction analysis of Hyperoside with *BChE*. D) Molecular interaction analysis of Kaempferol-3-O-glucoside with *BChE*.

for 100 ns to analyze the complexes formed between seven different bacterial target proteins and natural compounds. The structural and interactional stability of the systems was evaluated using a variety of criteria, including RMSD, RMSF, SASA, minimum distance, and hydrogen bond (Hbond) criteria.

The conformational stability of the complexes was assessed based on the RMSD values calculated relative to the protein backbone. In the *A. baumannii* EPSP synthase_Rutin complex, the RMSD values remained low in variance and stable throughout the simulation, indicating structurally reliable binding. Conversely, in the *A. baumannii* OXA-

231_Isorhamnetin complex, although RMSD values were initially stable, minor fluctuations were observed during the mid-phase of the simulation, suggesting some structural changes over time. The *A. baumannii* OXA-231_Quercetin complex exhibited consistent stability, as evidenced by a reliably stable RMSD profile, indicative of structural robustness. In the *L. monocytogenes* InlA_Delphinidin-3,5-diglucoside complex, the RMSD curve exhibited significant fluctuations, indicating that the system failed to form a stable structure after binding. For the *L. monocytogenes* MurA1_Delphinidin-3,5-diglucoside complex, the RMSD values were initially stable but increased after 60 ns, indicating a late-stage conformational change in the system. In the *S. aureus* MurE-Catechin and *S. aureus* MurE-Isoquercitrin complexes, the low-variance and stable RMSD profiles indicated that the systems remained structurally balanced throughout the binding process (Fig. 2A).

The mobility of the complexes at the residue level was evaluated using RMSF analysis. This analysis is particularly critical for determining the flexibility of amino acids located in the ligand-binding region. In the *A. baumannii* EPSP synthase_Rutin complex, residues corresponding to the binding site exhibited low RMSF values, indicating that the ligand was tightly bound to the target region and that this region was structurally stabilized. In the *A. baumannii* OXA-231_Isorhamnetin complex, low to moderate RMSF values were observed in the binding site, suggesting that the local stability of the system was largely preserved. In the complex formed by *A. baumannii* OXA-231_Quercetin binding, residues in the binding region showed low RMSF values, further supporting conformational stability. Conversely, the *L. monocytogenes* InlA_Delphinidin-3,5-diglucoside complex exhibited elevated RMSF values in the binding region, indicative of suboptimal binding and structural flexibility. In the *L. monocytogenes* MurA1_Delphinidin-3–5-diglucoside complex, the binding site initially displayed a low RMSF profile, supporting strong binding during the first 80 ns. However, a distance increase observed in the final stage of the simulation suggests the onset of structural relaxation. In the *S. aureus* MurE_Catechin and *S. aureus* MurE_Isoquercitrin complexes, the binding regions exhibited low RMSF values, indicating preserved structural integrity and stabilization of the target site by the ligands. This observation is particularly evident in the Isoquercitrin complex, where the mobility of residues within the binding site remained at a minimum level (Fig. 2B).

SASA analyses were conducted to assess the extent of ligand embedding within the protein surface following binding. In the *A. baumannii* EPSP synthase_Rutin complex, a decrease in SASA value over time was observed, indicating that the system underwent a process of compaction. A comparable decline in SASA values was observed following Quercetin binding to *A. baumannii* OXA-231, indicating that the ligand was seamlessly integrated into the binding region. A comparable decrease in SASA values was observed following Quercetin

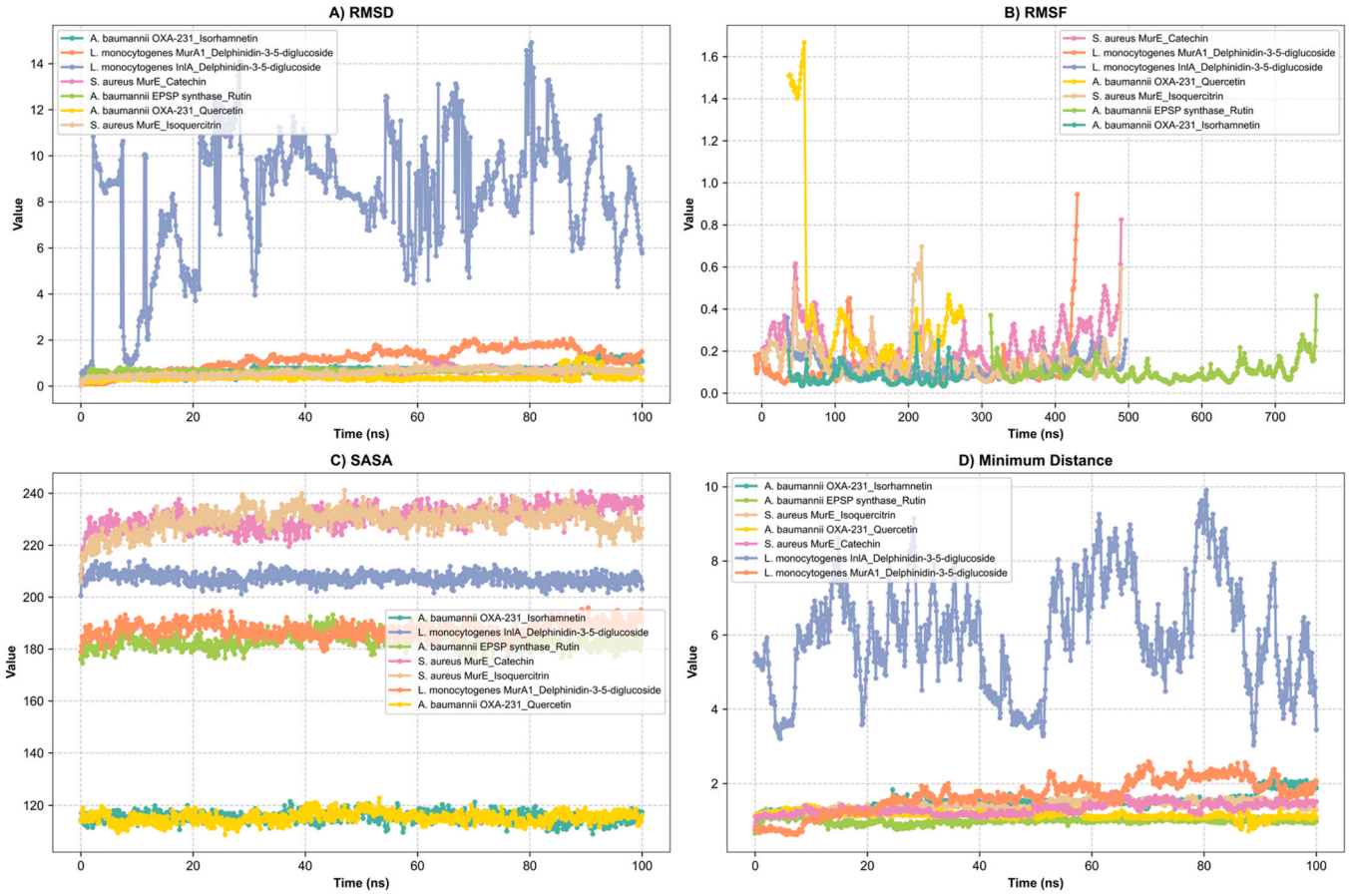

Fig. 2. Presentation of molecular dynamics simulations in graphical form; A) RMSD of the *A. baumannii-EPSP Synthase_Rutin, A. baumannii-OXA231_Isorhamnetin, A. baumannii-OXA231_Quercetin, L. monocytogenes-InlA_Delphinidin-3–5-diglucoside, L. monocytogenesMurA1_Delphinidin-3–5-diglucoside,* and *S. aureus-MurE_Catechin* complexes. B) RMSF of the *A. baumannii-EPSP Synthase_Rutin, A. baumannii-OXA231_Isorhamnetin, A. baumannii-OXA231_Quercetin, L. monocytogenes-InlA_Delphinidin-3–5-diglucoside, L. monocytogenes MurA1_Delphinidin-3–5-diglucoside,* and *S. aureus-MurE_Catechin complexes*. C) Solvent accessibility of the *A. baumannii-EPSP Synthase_Rutin, A. baumannii-OXA231_Isorhamnetin, A. baumannii-OXA231_Quercetin, L. monocytogenes-InlA_Delphinidin-3–5-diglucoside, L. monocytogenes MurA1_Delphinidin-3–5-diglucoside,* and *S. aureus-MurE_Catechin complexes*. D) Minimum distance of the *A. baumannii-EPSP Synthase_Rutin, A. baumannii-OXA231_Isorhamnetin, A. baumannii-OXA231_Quercetin, L. monocytogenes-InlA_Delphinidin-3–5-diglucoside, L. monocytogenes MurA1_Delphinidin-3–5-diglucoside,* and *S. aureus-MurE_Catechin complexes*.

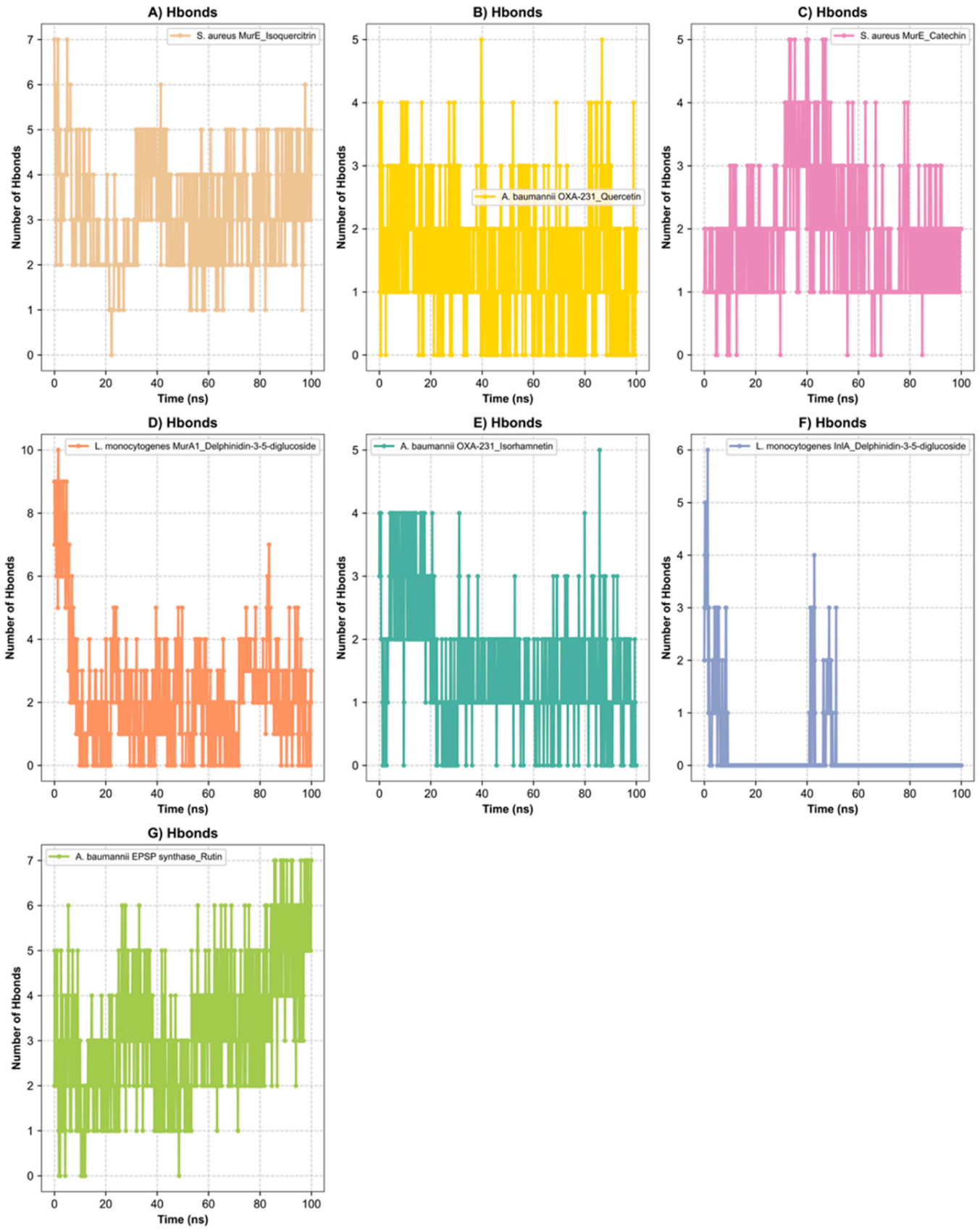

Fig. 3. Hydrogen bonds analysis. A) Hydrogen bonds of the *A. baumannii-EPSP Synthase_Rutin* complex. B) Hydrogen bonds of the *A. baumannii-OXA231_Isorhamnetin* complex. C) Hydrogen bonds of the *A. baumannii-OXA231_Quercetin* complex. D) Hydrogen bonds of the *L. monocytogenes-InlA_Delphinidin-3–5-diglucoside* complex. E) Hydrogen bonds of the *L. monocytogenesMurA1_Delphinidin-3–5-diglucoside* complex. F) Hydrogen bonds of the *S. aureus-MurE_Catechin* complex.

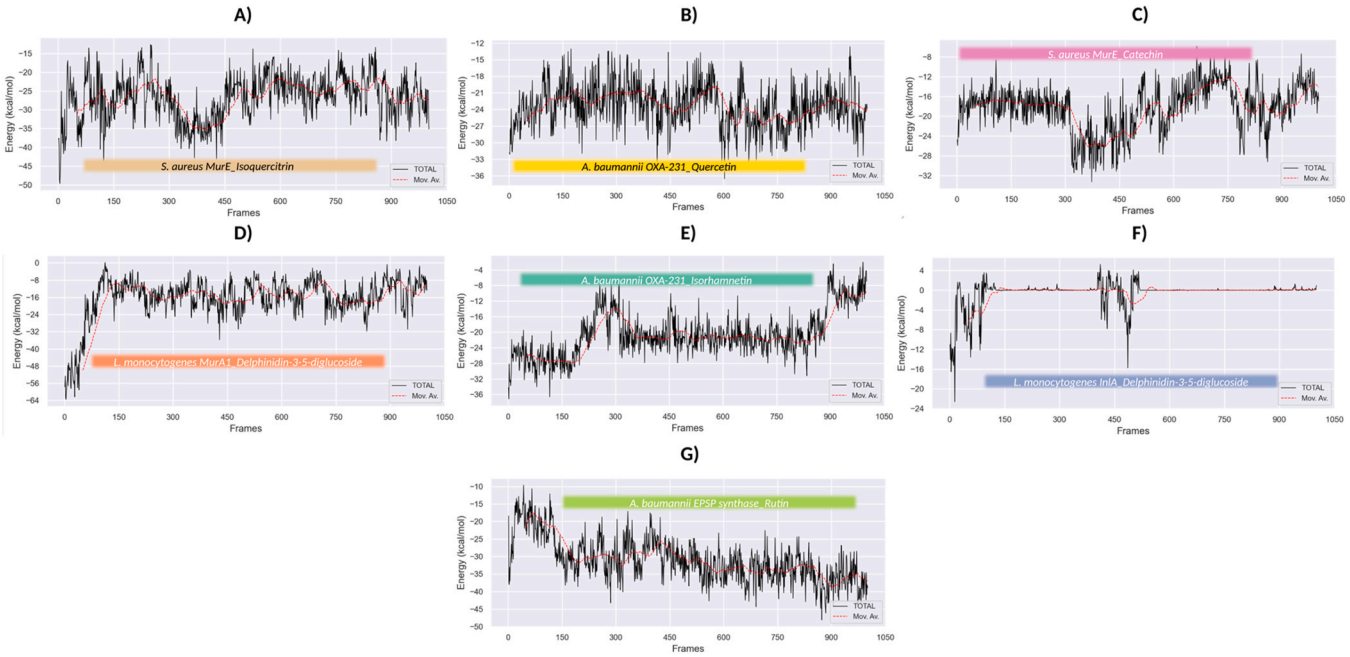

Fig. 4. MMPBSA analysis. A) Hydrogen bonds of the *A. baumannii-EPSP Synthase_Rutin* complex. B) Hydrogen bonds of the *A. baumannii-OXA231_Isorhamnetin* complex. C) Hydrogen bonds of the *A. baumannii-OXA231_Quercetin* complex. D) Hydrogen bonds of the *L. monocytogenes-InlA_Delphinidin-3–5-diglucoside* complex. E) Hydrogen bonds of the *L. monocytogenesMurA1_Delphinidin-3–5-diglucoside* complex. F) Hydrogen bonds of the *S. aureus-MurE_Catechin* complex.

binding to *A. baumannii* OXA-231, suggesting that the ligand was well integrated into the binding region. In the *S. aureus* MurE_Isoquercitrin complex, SASA values also decreased after binding, reflecting a tighter encapsulation of the protein by the ligand. Conversely, the *A. baumannii* OXA-231_Isorhamnetin complex exhibited variable SASA values, suggesting a less stable binding profile at the protein surface. In the *S. aureus* MurE_Catechin complex, SASA values remained low throughout the simulation but exhibited a slight increase over time, suggesting that the ligand was partially embedded within the binding site. In the *L. monocytogenes* MurA1_Delphinidin-3–5-diglucoside complex, SASA values remained low during the first 80 ns but showed a notable increase in the final 20 ns period. This observation indicates that while the ligand initially occupied the binding region, it gradually dissociated toward the surface in the later stages of the simulation. Conversely, in the *L. monocytogenes* InlA_Delphinidin-3–5-diglucoside complex, SASA values remained consistently high throughout the simulation, thereby confirming the absence of effective binding (Fig. 2C).

In the minimum distance analysis, the binding distances between the ligand and the target protein were evaluated across different time intervals. In the *A. baumannii* EPSP synthase_Rutin complex, the binding distance was initially measured at 0.98 Å, with slight fluctuations observed in the average values. During the 80–100 ns interval, the distance tightened again, returning to approximately 1.00 Å, indicating that the system generally maintained stable binding. In the *A. baumannii* OXA-231_Isorhamnetin complex, the initial distance was 1.19 Å and gradually increased over time, reaching 1.53 Å in the final period. This trend reflects a progressively loosening binding profile. In the *A. baumannii* OXA-231_Quercetin complex, the binding distance increased during the mid-simulation period but decreased again in the 80–100 ns interval, suggesting that the system re-stabilized and recovered its binding interaction at later stages. In the *L. monocytogenes* InlA_Delphinidin-3–5-diglucoside complex, the binding distance remained high from the beginning (5.32 Å), reaching 6.18 Å in the final period. These findings indicate that the complex failed to achieve effective binding throughout the simulation. In the *L. monocytogenes* MurA1_Delphinidin-3–5-diglucoside complex, the binding distance began at approximately 0.76 Å and remained stable until the 80-nanometer mark. Thereafter, it abruptly increased to 1.76 Å during the 80–100-nanometer period. These results suggest a disruption of binding in the later stages of the simulation. In the *S. aureus* MurE_Catechin complex, the binding distance commenced at 1.11 Å and exhibited a gradual and steady increase, reaching 1.34 Å in the final period. This suggests that although the interaction slightly loosened over time, it was largely maintained. In the *S. aureus* MurE_Isoquercitrin complex, the binding distance exhibited a consistent and gradual increase throughout the simulation, reaching 1.42 Å in the 80–100 ns interval. This trend suggests that although the initial binding was strong, the interaction gradually weakened over time (Fig. 2D).

The chemical binding stability of the ligands on the protein surface was assessed through the implementation of hydrogen bond analyses. In the *S. aureus* MurE_Isoquercitrin complex, the number of hydrogen bonds was determined to be 3, and the bond count was preserved throughout the simulation (Fig. 3A). A similar trend was observed in the *A. baumannii* OXA-231_Quercetin complex, where the average number of hydrogen bonds decreased from 2 to 1 over time (Fig. 3B). In the *S. aureus* MurE_Catechin complex, the average number of hydrogen bonds remained relatively stable at 2 (Fig. 3C). In the *L. monocytogenes* MurA1_Delphinidin-3,5-diglucoside complex, the initially high number of hydrogen bonds (10) gradually decreased and dropped to 2 in the 80–100 ns period. This observation suggests that the chemical binding was disrupted in the late stage of the simulation (Fig. 3D). In contrast, the *A. baumannii* OXA-231_Isorhamnetin complex exhibited an average of 2 hydrogen bonds, which exhibited a downward trend over time (Fig. 3E). In the *L. monocytogenes* InlA_Delphinidin-3,5-diglucoside complex, the number of hydrogen bonds was found to be minimal, exhibiting a decline to nearly zero during the 80–100 ns interval (Fig. 3F). In the A. *baumannii* EPSP synthase_Rutin complex, the average number of hydrogen bonds was 3 and exhibited an increasing trend over time. This upward trend indicates that the system became progressively stabilized (Fig. 3G).

The binding free energy profiles of the protein-ligand complexes were evaluated over the 100 ns simulation period using the molecular mechanics MM/PBSA method (Fig. 4). In the *A. baumannii* EPSP synthase_Rutin complex, the total energy profile decreased steadily over

time, indicating that the interaction became increasingly stable (Fig. 4A). In the *A. baumannii* OXA-231_Quercetin complex, the total binding energy remained relatively constant, with only minor fluctuations, suggesting a consistent interaction throughout the simulation (Fig. 4B). A similar trend was observed in the *S. aureus* MurE_Catechin complex, where fluctuations persisted throughout the simulation (Fig. 4C). Conversely, in the *A. baumannii* OXA-231–Isorhamnetin complex, a gradual increase in binding energy was observed over time, suggesting a weakening of the interaction (Fig. 4E). In the *L. monocytogenes* MurA1_Delphinidin-3–5-diglucoside complex, a sharp increase in total energy was detected, particularly in the second half of the simulation, suggesting that the complex became significantly destabilized (Fig. 4D). A similar trend was observed in the *L. monocytogenes* InlA_Delphinidin-3–5-diglucoside complex, which exhibited high and unstable energy values, indicative of weak binding affinity and dynamic instability (Fig. 3F). Conversely, the *S. aureus* MurE_Isoquercitrin complex demonstrated low and stable binding energy profiles, substantiating a robust and sustained interaction throughout the duration of the simulation (Fig. 3A).

4. Conclusion

Extracts of the plant species *T. nigrescens* were obtained with solvents of different polarity to extract the phytonutrients more efficiently and to obtain high-quality extracts. The chemical composition of the extracts was determined using the HPLC method, with delphinidin-3-galactose, hyperoside and ellagic acid dominating molecules. The influence of the polarity of the solvent was more evident in the antioxidant activity, where the extract obtained with 70 % ethanol as solvent dominated. In enzyme inhibitory activity, the ethyl acetate extract also showed strong enzyme inhibitory activity, assuming that the polarity of this solvent influenced the extraction of less polar molecules that contributed to the result obtained Furthermore, molecular docking and molecular dynamics simulations revealed the robust interaction profiles of rutin and isoquercitrin with bacterial targets, particularly *A. baumannii* EPSP synthase and *S. aureus* MurE. These complexes demonstrated low RMSD, RMSF and minimum distance high Hbond values, stable hydrogen bond networks, and favorable mean molecular potential and free energy of binding throughout 100 ns simulations, confirming their structural and energetic stability. Rutin, quercetin, catechin, kaempferol, isorhamenetin, delphindin-3-galactoside, ellagic acid, kaempferol-3-O-glucoside, hyperoside, and phloridzin exhibited relatively favorable docking affinities; however, they lacked consistent dynamic or energetic support. Furthermore, the investigation revealed that certain compounds exhibited noteworthy docking activity against selected standard enzymes, including amylase, AChE, and BChE, suggesting the possibility of multitarget effects. Although molecular dynamics simulations were not performed for these targets, the docking results warrant further investigation. The analysis of *T. nigrescens* revealed that it is able to inhibit mature biofilms or affect the metabolism of their sessile cells, with the inhibition rate reaching almost 60 %. Taken together, these results highlight the potential utility of *T. nigrescens* extracts for possible applications in the food or pharmaceutical industries, where the use of 70 % ethanol as a solvent for the extraction of bioactive compounds is justified from both an economic and environmental point of view.

CRediT authorship contribution statement

Giovanni Caprioli: Writing – original draft, Supervision, Methodology, Investigation, Conceptualization. **Mehmet Veysi Cetiz:** Writing – original draft, Visualization, Validation, Methodology, Investigation, Conceptualization. **Simone Angeloni:** Writing – original draft, Supervision, Methodology, Investigation, Conceptualization. **Laura Acquaticci:** Writing – original draft, Visualization, Methodology, Investigation, Conceptualization. **saka Enver:** Writing – review & editing, Writing – original draft, Methodology, Investigation. **Ismail Senkardes:** Validation, Resources, Methodology, Data curation. **Francesca Coppola:** Writing – review & editing, Writing – original draft, Supervision, Methodology, Investigation, Conceptualization. **Milena Terzic:** Writing – review & editing, Writing – original draft, Investigation, Funding acquisition, Conceptualization. **Florinda Fratianni:** Writing – review & editing, Writing – original draft, Methodology, Investigation, Conceptualization. **Andrei Mocan:** Writing – review & editing, Writing – original draft, Supervision, Investigation, Data curation, Conceptualization. **Filomena Nazzaro:** Writing – review & editing, Writing – original draft, Supervision, Methodology, Investigation, Conceptualization. **Gokhan Zengin:** Writing – review & editing, Writing – original draft, Supervision, Methodology, Investigation, Funding acquisition, Conceptualization. **Oleg Frumuzachi:** Writing – review & editing, Writing – original draft, Visualization, Investigation, Conceptualization.

Declaration of Competing Interest

The authors declare that they have no known competing financial interests or personal relationships that could have appeared to influence the work reported in this paper. The authors declare that there are no conflicts of interest.

Acknowledgments

This work was supported by the Ministry of Science, Technological Development and Innovation of the Republic of Serbia (contract no. 451–03–136/2025–03/200134).

Appendix A. Supporting information

Supplementary data associated with this article can be found in the online version at doi:10.1016/j.indcrop.2025.121484.

Data availability

Data will be made available on request.

References

Alexander, J.A.N., Chatterjee, S.S., Hamilton, S.M., Eltis, L.D., Chambers, H.F., Strynadka, N.C., 2018. Structural and kinetic analyses of penicillin-binding protein 4 (PBP4)-mediated antibiotic resistance in *Staphylococcus aureus*. J. Biol. Chem. 293, 19854–19865.

Almihyawi, R.A., Naman, Z.T., Al-Hasani, H.M., Muhseen, Z.T., Zhang, S., Chen, G., 2022. Integrated computer-aided drug design and biophysical simulation approaches to determine natural anti-bacterial compounds for *Acinetobacter baumannii*. Sci. Rep. 12, 6590.

Altamimi, J., Alfaris, N., Alshammari, G., Alagal, R., Aljabryn, D., Aldera, H., Alkhateeb, M., Yahya, M., 2020. Ellagic acid protects against diabetic cardiomyopathy in rats by stimulating cardiac silent information regulator 1 signaling. J. Physiol. Pharm. 71, 10.26402.

Angeles Flores, G., Cusumano, G., Zengin, G., Cetiz, M.V., Uba, A.I., Senkardes, I., Koyuncu, I., Yuksekdag, O., Kalyniukova, A., Emiliani, C., 2024. Using in vitro and in silico analysis to investigate the chemical profile and biological properties of *Polygonum istanbulicum* extracts. Plants 13, 3421.

Antunes, V.U., Llontop, E.E., Vasconcelos, F.Nd.C., López, de los Santos, Y., Oliveira, R. J., Lincopan, N., Farah, C.S., Doucet, N., Mittermaier, A., Favaro, D.C., 2019. Importance of the β5− β6 loop for the structure, catalytic efficiency, and stability of carbapenem-hydrolyzing class D β-lactamase subfamily OXA-143. Biochem 58, 3604–3616.

Badger, J., Chie-Leon, B., Logan, C., Sridhar, V., Sankaran, B., Zwart, P.H., Nienaber, V., 2012. Structure determination of LpxA from the lipopolysaccharide-synthesis pathway of *Acinetobacter baumannii*. Struct. Biol. Cryst. Commun. 68, 1477–1481.

Balkrishna, A., Sharma, N., Srivastava, D., Kukreti, A., Srivastava, S., Arya, V., 2024. Exploring the safety, efficacy, and bioactivity of herbal medicines: bridging traditional wisdom and modern science in healthcare. Future Integr. Med. 3, 35–49.

Baloglu, M.C., Ozer, L.Y., Pirci, B., Altunoglu, Y.C., Soomro, S.I., Zengin, G., Cetiz, M.V., Carradori, S., Cziáky, Z., Jekő, J., 2025. Decoding chemical profiles, biological functions, and medicinal properties of *Liquidambar orientalis* extracts through molecular modeling and bioinformatic methods. Food Front. 6, 1376–1408.

Barna, T.M., Khan, H., Bruce, N.C., Barsukov, I., Scrutton, N.S., Moody, P.C., 2001. Crystal structure of pentaerythritol tetranitrate reductase:"flipped" binding

geometries for steroid substrates in different redox states of the enzyme. J. Mol. Biol. 310, 433–447.
Belousoff, M.J., Eyal, Z., Radjainia, M., Ahmed, T., Bamert, R.S., Matzov, D., Bashan, A., Zimmerman, E., Mishra, S., Cameron, D., 2017. Structural basis for linezolid binding site rearrangement in the *Staphylococcus aureus* ribosome. MBio 8, e00395-17.
Bublitz, M., Holland, C., Sabet, C., Reichelt, J., Cossart, P., Heinz, D.W., Bierne, H., Schubert, W.-D., 2008. Crystal structure and standardized geometric analysis of InlJ, a listerial virulence factor and leucine-rich repeat protein with a novel cysteine ladder. J. Mol. Biol. 378, 87–96.
Budzyńska, A., Sadowska, B., Więckowska-Szakiel, M., Micota, B., Stochmal, A., Jędrejek, D., Pecio, Ł., Różalska, B., 2014. Saponins of *Trifolium* spp. aerial parts as modulators of *Candida albicans* virulence attributes. Molecules 19, 10601–10617.
Cankaya, I.I., Somuncuoglu, E.I., 2021. Potential and prophylactic use of plants containing saponin-type compounds as antibiofilm agents against respiratory tract infections. Evid. Based Complement. Altern. Med. 2021 (1), 6814215.
Ceci, C., Lacal, P.M., Tentori, L., De Martino, M.G., Miano, R., Graziani, G., 2018. Experimental evidence of the antitumor, antimetastatic and antiangiogenic activity of ellagic acid. Nutrients 10, 1756.
Cetiz, M.V., Ahmed, S., Zengin, G., Sinan, K.I., Emre, G., Dolina, K., Kalyniukova, A., Uba, A.I., Koyuncu, I., Yuksekdag, O., 2025. Bioinformatic and experimental approaches to uncover the bio-potential of *Mercurialis annua* extracts based on chemical constituents. J. Mol. Liq. 427, 127390.
Cetiz, M.V., Isah, M., Ak, G., Bakar, K., Himidi, A.A., Mohamed, A., Glamočlija, J., Nikolić, F., Gašic, U., Cespedes-Acuna, C.L., 2024. Exploring of chemical profile and biological activities of three *Ocimum* species from Comoros islands: a combination of in vitro and in silico insights. Cell Bioch. Funct. 42, e70000.
Chiavaroli, A., Libero, M.L., Di Simone, S.C., Acquaviva, A., Nilofar, Recinella, L., Leone, S., Brunetti, L., Cicia, D., Izzo, A.A., Orlando, G., Zengin, G., Uba, A.I., Cakilcioğlu, U., Mukemre, M., Elkiran, O., Menghini, L., Ferrante, C., 2023. Adding new scientific evidences on the pharmaceutical properties of *Pelargonium quercetorum* agnew extracts by using in vitro and in silico approaches. Plants 12, 1132.
Chopra, A.S., Lordan, R., Horbańczuk, O.K., Atanasov, A.G., Chopra, I., Horbańczuk, J. O., Jóźwik, A., Huang, L., Pirgozliev, V., Banach, M., 2022. The current use and evolving landscape of nutraceuticals. Pharmacol. Res. 175, 106001.
Demirkiran, O., Sabudak, T., Ozturk, M., Topcu, G., 2013. Antioxidant and tyrosinase inhibitory activities of flavonoids from *Trifolium nigrescens* subsp. *petrisavi*. J. Agric. Food Chem. 61, 12598–12603.
Dileep, K.V., Ihara, K., Mishima-Tsumagari, C., Kukimoto-Niino, M., Yonemochi, M., Hanada, K., Shirouzu, M., Zhang, K.Y.J., 2022. Crystal structure of human acetylcholinesterase in complex with tacrine: implications for drug discovery. Int. J. Biol. Macromol. 210, 172–181.
Elkordy, A.A., Haj-Ahmad, R.R., Awaad, A.S., Zaki, R.M., 2021. An overview on natural product drug formulations from conventional medicines to nanomedicines: past, present and future. J. Drug Deliv. Sci. Technol. 63, 102459.
Fratianni, F., Amato, G., d'Acierno, A., Ombra, M.N., De Feo, V., Coppola, R., Nazzaro, F., 2023. In vitro prospective healthy and nutritional benefits of different *Citrus* monofloral honeys. Sci. Rep. 13, 1088.
Frumuzachi, O., Flanagan, A., Rohn, S., Mocan, A., 2025. The dichotomy between functional and functionalized foods – A critical characterization of concepts. Food Res. Int. 208, 116173.
Grochowski, D.M., Uysal, S., Aktumsek, A., Granica, S., Zengin, G., Ceylan, R., Locatelli, M., Tomczyk, M., 2017. In vitro enzyme inhibitory properties, antioxidant activities, and phytochemical profile of *Potentilla thuringiaca*. Phytochem. Lett. 20, 365–372.
Hampele, I.C., D'Arcy, A., Dale, G.E., Kostrewa, D., Nielsen, J., Oefner, C., Page, M.G., Schönfeld, H.-J., Stüber, D., Then, R.L., 1997. Structure and function of the dihydropteroate synthase from Staphylococcus aureus. Elsevier 21–30.
Hanganu, D., Benedec, D., Vlase, L., Olah, N., Damian, G., Silaghi-Dumitrescu, R., Mot, A. C., Toma, C.C., 2017. Polyphenolic profile and antioxidant and antibacterial activities from two *Trifolium* species. Farmacia 65, 449–453.
Jo, S., Kim, T., Iyer, V.G., Im, W., 2008. CHARMM-GUI: a web-based graphical user interface for CHARMM. J. Comp. Chem. 29, 1859–1865.
June, C.M., Muckenthaler, T.J., Schroder, E.C., Klamer, Z.L., Wawrzak, Z., Powers, R.A., Szarecka, A., Leonard, D.A., 2016. The structure of a doripenem-bound OXA-51 class D β-lactamase variant with enhanced carbapenemase activity. Protein Sci. 25, 2152–2163.
Kaitany, K.-C.J., Klinger, N.V., June, C.M., Ramey, M.E., Bonomo, R.A., Powers, R.A., Leonard, D.A., 2013. Structures of the class D carbapenemases OXA-23 and OXA-146: mechanistic basis of activity against carbapenems, extended-spectrum cephalosporins, and aztreonam. Antimicrob. Agents Chemother. 57, 4848–4855.
Kaurinovic, B., Popovic, M., Vlaisavljevic, S., Schwartsova, H., Vojinovic-Miloradov, M., 2012. Antioxidant profile of *Trifolium pratense* L. Molecules 17, 11156–11172.
Keith, E., 2013. *Trifolium nigrescens* (Fabaceae), new to the Texas flora. Phytoneuron 32, 1–6.
Keskin, M., 2024. Novelties in the genus *Trifolium* in Türkiye. Front. Life Sci. Rt. 5, 140–154.
Khan, A.V., Ahmed, Q.U., Shukla, I., Khan, A.A., 2012. Antibacterial activity of leaves extracts of *Trifolium alexandrinum* Linn. against pathogenic bacteria causing tropical diseases. Asian Pac. J. Trop. Biomed. 2, 189–194.
Khan, R.J., Singh, E., Jha, R.K., Kumar, A., Bhati, S.K., Zia, M.P., Jain, M., Singh, R.P., Muthukumaran, J., Singh, A.K., 2023. Identification and prioritization of potential therapeutic molecules against LpxA from *Acinetobacter baumannii*–A computational study. Curr. Res. Struct. Biol. 5, 100096.
Khorasani Esmaeili, A., Mat Taha, R., Mohajer, S., Banisalam, B., 2015. Antioxidant activity and total phenolic and flavonoid content of various solvent extracts from in vivo and in vitro grown *Trifolium pratense* L.(Red Clover). BioMed. Res. Int. 2015, 643285.
Kicel, A., Wolbiś, M., 2013. Phenolic content and DPPH radical scavenging activity of the flowers and leaves of *Trifolium repens*. Nat. Prod. Comm. 8, 99–102.
Kolodziejczyk-Czepas, J., 2012. *Trifolium* species-derived substances and extracts—Biological activity and prospects for medicinal applications. J. Ethnopharmacol. 143, 14–23.
Kolodziejczyk-Czepas, J., 2016. *Trifolium* species – the latest findings on chemical profile, ethnomedicinal use and pharmacological properties. J. Pharm. Pharm. 68, 845–861.
Kolodziejczyk-Czepas, J., Nowak, P., Kowalska, I., Stochmal, A., 2014. Biological activity of clovers–Free radical scavenging ability and antioxidant action of six *Trifolium* species. Pharm. Biol. 52, 1308–1314.
Korpayev, S., Zengin, G., Ak, G., Glamočlija, J., Soković, M., Aničić, N., Gašić, U., Stojković, D., Agamyradov, M., Cetiz, M.V., 2025. Integration of *in* vitro and *in* silico results from chemical and biological assays of *Rheum turkestanicum* and *Calendula officinalis* flower extracts. Food Sci. Nutr. 13, e4663.
Köster, S., Van Pee, K., Hudel, M., Leustik, M., Rhinow, D., Kühlbrandt, W., Chakraborty, T., Yildiz, Ö., 2014. Crystal structure of listeriolysin O reveals molecular details of oligomerization and pore formation. Nat. Commun. 5, 3690.
Kulen, M., Lindgren, M., Hansen, S., Cairns, A.G., Grundstrom, C., Begum, A., Van Der Lingen, I., Brannstrom, K., Hall, M., Sauer, U.H., 2018. Structure-based design of inhibitors targeting PrfA, the master virulence regulator of *Listeria monocytogenes*. J. Med. Chem. 61, 4165–4175.
Lim, X.Y., Teh, B.P., Tan, T.Y.C., 2021. Medicinal plants in COVID-19: potential and limitations. Front. Pharm. 12, 611408.
Liu, R., Li, J., Cheng, Y., Huo, T., Xue, J., Liu, Y., Liu, J., Chen, X., 2015. Effects of ellagic acid-rich extract of pomegranates peel on regulation of cholesterol metabolism and its molecular mechanism in hamsters. Food Funct. 6, 780–787.
Llorent-Martínez, E.J., Yagi, S., Zengin, G., Cetiz, M.V., Uba, A.I., Yuksekdag, O., Akgul, B.H., Yildiztugay, E., Koyuncu, I., 2025. Characterization of the chemical profiles and biological activities of *Thesium bertramii* Azn. Extracts using a combination of in vitro, in silico, and network pharmacology methods. Fitoterapia 180, 106329.
Lu, J., Patel, S., Sharma, N., Soisson, S.M., Kishii, R., Takei, M., Fukuda, Y., Lumb, K.J., Singh, S.B., 2014. Structures of kibdelomycin bound to *Staphylococcus aureus* GyrB and ParE showed a novel U-shaped binding mode. ACS Chem. Biol. 9, 2023–2031.
Maier, J.A., Martinez, C., Kasavajhala, K., Wickstrom, L., Hauser, K.E., Simmerling, C., 2015. ff14SB: improving the accuracy of protein side chain and backbone parameters from ff99SB. J. Chem. The. Comp. 11, 3696–3713.
Mngoma, M.F., Magwaza, L.S., Mditshwa, A., Tesfay, S.Z., Mkhwanazi, B.N., Nkomo, M. A., 2025. Comparative profiling of bioactive compounds and antioxidant activity of extracts from selected medicinal plants: implications for mitigating obesity-related inflammation. South Afr. J. Bot. 181, 162–171.
Moser, J., Gerstel, B., Meyer, J.E., Chakraborty, T., Wehland, J., Heinz, D.W., 1997. Crystal structure of the phosphatidylinositol-specific phospholipase C from the human pathogen *Listeria monocytogenes*. J. Mol. Biol. 273, 269–282.
Najmi, A., Nikrad, N., Sarghein, M.G., Alizadeh, M., 2024. Ellagic acid supplementation on oxidative stress, antioxidative capacity and inflammation biomarkers: a systematic review and dose–response meta-analysis of randomized controlled trials. J. Funct. Foods 122, 106492.
Nazzaro, F., Ombra, M.N., Coppola, F., De Giulio, B., d'Acierno, A., Coppola, R., Fratianni, F., 2024. Antibacterial activity and prebiotic properties of six types of lamiaceae honey. Antibiotics 13, 868.
Ngangom, L., Venugopal, D., Pandey, N., Kumar, N., 2023. In-silico screening and identification of potential bioactive compounds of *Trifolium repens* against pathogenic bacterial target proteins. Mater. Today 73, 142–150.
Njoya, E.M., 2021. Medicinal plants, antioxidant potential, and cancer. Cancer. Elsevier, pp. 349–357.
Ooi, A., Hussain, S., Seyedarabi, A., Pickersgill, R.W., 2006. Structure of internalin C from *Listeria monocytogenes*. Biol. Crystallogr 62, 1287–1293.
Pakharukova, N., Tuittila, M., Paavilainen, S., Malmi, H., Parilova, O., Teneberg, S., Knight, S.D., Zavialov, A.V., 2018. Structural basis for *Acinetobacter baumannii* biofilm formation. Proc. Natl. Acad. Sci. 115, 5558–5563.
Park, J.S., Lee, W.C., Yeo, K.J., Ryu, K.-S., Kumarasiri, M., Hesek, D., Lee, M., Mobashery, S., Song, J.H., Kim, S.I., 2012. Mechanism of anchoring of OmpA protein to the cell wall peptidoglycan of the gram-negative bacterial outer membrane. FASEB J. 26, 219.
Pejin, B., Ciric, A., Dimitric Markovic, J., Glamoclija, J., Nikolic, M., Sokovic, M., 2017. An insight into anti-biofilm and anti-quorum sensing activities of the selected anthocyanidins: the case study of *Pseudomonas aeruginosa* PAO1. Nat. Prod. Res. 31, 1177–1180.
Pourhajibagher, M., Javanmard, Z., Bahador, A., 2024. In vitro antibacterial activity of photoactivated flavonoid glycosides against *Acinetobacter baumannii*. AMB Express 14, 119.
Ríos, J.-L., Giner, R.M., Marín, M., Recio, M.C., 2018. A pharmacological update of ellagic acid. Plant. Med. 84, 1068–1093.
Rosenberry, T.L., Brazzolotto, X., Macdonald, I.R., Wandhammer, M., Trovaslet-Leroy, M., Darvesh, S., Nachon, F., 2017. Comparison of the binding of reversible inhibitors to human butyrylcholinesterase and acetylcholinesterase: a crystallographic, kinetic and calorimetric study. Molecules 22, 2098.
Salem, M.A., Salama, M.M., Ezzat, S.M., Hashem, Y.A., 2022. Comparative metabolite profiling of four polyphenol rich Morus leaves extracts in relation to their antibiofilm activity against *Enterococcus faecalis*. Sci. Rep. 12, 20168.
Sarker, S.D., Nahar, L., Kumarasamy, Y., 2007. Microtitre plate-based antibacterial assay incorporating resazurin as an indicator of cell growth, and its application in the in vitro antibacterial screening of phytochemicals. Methods 42, 321–324.

Sathasivam, R., Kim, N.S., Lim, J., Yang, S.H., Kim, B., Park, H.W., Kim, J.K., Park, S.U., 2025. Comprehensive analysis of primary and secondary metabolites and antioxidant activities provides insights into metabolic profiling of different organs of *Pimpinella brachycarpa* Nakai. Food Chem. 468, 142394.

Schubert, W.-D., Urbanke, C., Ziehm, T., Beier, V., Machner, M.P., Domann, E., Wehland, J., Chakraborty, T., Heinz, D.W., 2002. Structure of internalin, a major invasion protein of *Listeria monocytogenes*, in complex with its human receptor E-cadherin. Cell 111, 825–836.

Slinkard, K., Singleton, V.L., 1977. Total phenol analysis: automation and comparison with manual methods. Am. J. Enol. Viticult 28, 49–55.

Smith, C.A., Antunes, N.T., Toth, M., Vakulenko, S.B., 2014. Crystal structure of carbapenemase OXA-58 from *Acinetobacter baumannii*. Antimicrob. Agents Chemother. 58, 2135–2143.

Sultana, S., Foster, K., Lim, L.Y., Hammer, K., Locher, C., 2022. A review of the phytochemistry and bioactivity of clover honeys (*Trifolium* spp.). Foods 11, 1901.

Sutton, K.A., Breen, J., Russo, T.A., Schultz, L.W., Umland, T.C., 2016. Crystal structure of 5-enolpyruvylshikimate-3-phosphate (EPSP) synthase from the ESKAPE pathogen *Acinetobacter baumannii*. Struct. Biol. Cryst. Commun. 72, 179–187.

Tava, A., Pecio, Ł., Lo Scalzo, R., Stochmal, A., Pecetti, L., 2019. Phenolic content and antioxidant activity in *Trifolium* germplasm from different environments. Molecules 24, 298.

Trott, O., Olson, A.J., 2010. AutoDock Vina: improving the speed and accuracy of docking with a new scoring function, efficient optimization, and multithreading. J. Comput. Chem. 31, 455–461.

Valdés-Tresanco, M.S., Valdés-Tresanco, M.E., Valiente, P.A., Moreno, E., 2021. gmx_MMPBSA: a new tool to perform end-state free energy calculations with GROMACS. J. Chem. Theory Comp. 17, 6281–6291.

Wang, L., Shao, X., Zhong, T., Wu, Y., Xu, A., Sun, X., Gao, H., Liu, Y., Lan, T., Tong, Y., 2021. Discovery of a first-in-class CDK2 selective degrader for AML differentiation therapy. Nat. Chem. Biol. 17, 567–575.

Yagi, S., Cetiz, M.V., Zengin, G., Bakar, K., Himidi, A.A., Mohamed, A., Skorić, M., Glamočlija, J., Gašić, U., 2025. Novel natural candidates for replacing synthetic additives in nutraceutical and pharmaceutical areas: Two *Senna* Species (*S. alata* (L.) Roxb. and *S. occidentalis* (L.) Link). Food Sci. Nutr. 13, e4705.

Yildirim, M.A., Sevinc, B., Paydas, S., Karaselek, M.A., Duran, T., Kuccukturk, S., Vatansev, H., Cetiz, M.V., Caprioli, G., Acquaticci, L., 2025. Exploring the anticancer potential of *Dianthus orientalis* in pancreatic cancer: a molecular and cellular study. Food Biosci. 66, 106183.

Zengin, G., Uba, A.I., Abul, N., Gulcin, I., Koyuncu, I., Yuksekdag, O., Ponnaiya, S.K.M., Tessappan, S., Nazzaro, F., Fratianni, F., 2024. A multifunctional natural treasure based on a “one stone, many birds” strategy for designing health-promoting applications: *Tordylium apulum*. Food Biosci. 62, 105088.

Zhang, Y., Lin, Y., Huang, L., Tekliye, M., Rasheed, H.A., Dong, M., 2020. Composition, antioxidant, and anti-biofilm activity of anthocyanin-rich aqueous extract from purple highland barley bran. LWT 125, 109181.